The Thesis Committee for Nicholas Patrick Ettinger
Certifies that this is the approved version of the following thesis:

Carbonate Platform Demise and Recovery at The Toarcian Oceanic Anoxic Event: High-Resolution Data From the Adriatic Carbonate Platform

APPROVED BY
SUPERVISING COMMITTEE:

Supervisor:

Rowan C. Martindale

Co-Supervisor:

Charles Kerans

Toti E. Larson

Carbonate Platform Demise and Recovery at The Toarcian Oceanic Anoxic Event: High-Resolution Data From the Adriatic Carbonate Platform

by

Nicholas Patrick Ettinger, B.S.

Thesis

Presented to the Faculty of the Graduate School of

The University of Texas at Austin

in Partial Fulfillment

of the Requirements

for the Degree of

Master of Science in Geological Sciences

The University of Texas at Austin

May, 2017

Dedication

D.F.S.

Acknowledgements

I owe a great deal to Dr. Charles Kerans for showing me more carbonate rocks than I could have ever dreamed of, and for both directly and indirectly inspiring the way I think as a geologist. Thank you to Dr. Noel James for instilling in me a love for carbonates, to Dr. Jean Hsieh for giving me my first shot at proving myself a carbonate geologist, to Dr. Toti Larson for convincing me that sometimes I can also be a geochemist, and to Dr. Rowan Martindale for opening the doors to the University of Texas at Austin for me.

This thesis has greatly benefited from the intellectual, field, and laboratory-based support of Dr, Adrijan Košir, and from the laboratory support of Dr. Alyson Thibodeau. Funding was provided by the University of Texas at Austin, Jackson School of Geosciences, the Slovenian Academy of Sciences, the American Association of Petroleum Geologists (AAPG), and the Society for Sedimentary Geology (SEPM). Thank you to Sean Kacur for assistance with lab work at the University of Texas at Austin, and to my graduate school friends for the many productive discussions that this research has benefited from.

Abstract

Carbonate Platform Demise and Recovery at The Toarcian Oceanic Anoxic Event: High-Resolution Data From the Adriatic Carbonate Platform

Nicholas Patrick Ettinger, M.S. Geo. Sci.

The University of Texas at Austin, 2017

Supervisor: Rowan C. Martindale

Co-Supervisor: Charles Kerans

The sedimentological, stratigraphic, and geochemical signature of the Toarcian Oceanic Anoxic Event (OAE) on the Bahamian-style, Adriatic Carbonate Platform of Southern Europe is examined here. New stratigraphic sections correlated to previously published data show that a healthy and diverse metazoan carbonate factory characterized the flat-topped platform prior to the onset of the OAE. Carbon isotopes of marine organic matter and bulk carbonate, as well as trace element data (V, Ni, Mo, Mn, Hg) were used to identify the stratigraphic location of the OAE on the outer platform. A negative organic carbon isotope excursion of -2.2‰ coincident with enrichments in Mo and Fe was used to correlate to time equivalent strata in both the inner platform and adjacent basin. The onset of the OAE heralded a carbonate factory collapse on the outer platform that was driven by deoxygenation, eutrophication, and possibly ocean acidification. At

the same time, a shallow intrashelf basin developed, while the adjacent deep-water basin accumulated black shales. The cessation of carbonate production throughout the OAE yielded a significant drowning unconformity on the outer platform as sea-level continued to rise, while restricted, organic-rich mudstones accumulated on the inner platform under a euxinic regime. Recovery of carbonate production is characterized mainly by calcitic fauna and ooids. By the Middle Jurassic, ooids generated on the outer margin spilled into the adjacent basin forming a thick deep-water oolitic fan, and they prograded to the inner platform, reestablishing a flat-topped carbonate platform.

Table of Contents

List of Tables

List of Figures

INTRODUCTION

Oceanic Anoxic Events (OAEs) have been shown to have a strong influence on the deposition of organic carbon-rich (black) shales and the reorganization of carbonate factories throughout geologic time (Jenkyns, 2010; Danise et al., 2013; Phelps et al., 2014, 2015). The Lower Jurassic Toarcian OAE, in particular, was a geologically brief episode associated with globally enhanced organic carbon burial (Jenkyns, 2010) and the loss of approximately 5% of all marine families and 26% of genera (Danise et al., 2013). The emplacement of the Karoo-Ferrar-Chon Aike Large Igneous Province is coincident with black shale deposition and environmental perturbations of the late Pliensbachian-early Toarcian (Burgess et al., 2015) and as such is generally accepted as the trigger for both the OAE and the preceding late Pliensbachian-early Toarcian extinction event (Littler et al., 2010; Caruthers et al., 2013; Bodin et al., 2016). Whether the mechanism was by the rapid introduction of volatiles and particulates (CO_2, CH_4, SO_4, Cl, F, S, etc.) into the ocean-atmosphere system via direct subaerial volcanism (Pálfy & Smith, 2000; Suan et al., 2008), degassing following intrusive contact metamorphism of carbon-rich host rocks (e.g. Svensen et al., 2009; Burgess et al., 2015) or by the destabilization of continental methane hydrate reservoirs (Hesselbo et al., 2000), the Toarcian OAE was, in essence, a major global carbon cycle perturbation that had profound and far reaching impacts on the Earth's ocean-atmosphere system. This perturbation is defined by a global negative excursion in the $d^{13}C$ of marine carbonate and organic matter (e.g. Bodin et al., 2016; Müller et al., 2017) and in terrestrial organics (Hesselbo et al., 2007; Littler et al., 2010).

A cascade of global environmental changes are associated with the Pliensbachian-Toarcian event and the Toarcian OAE, including, but not limited to, a massive increase in

atmospheric pCO_2 [1,000 ppm increase in CO_2 in the Pliensbachian and 2,000 ppm increase in the early Toarcian (Steinthorsdottir & Vajda, 2015)], an approximate 7°C spike in sea-surface temperatures in the NW Tethys (Suan et al., 2010), and a 500-800% increase in the rate of continental weathering during the OAE (Cohen et al., 2004; Brazier et al., 2015). These drastic changes ultimately led to ocean stratification and the expansion of anoxia (Mattioli et al., 2004; Gröcke et al., 2011; Suan et al., 2016), as well as a short-lived lowering of carbonate saturation states (Hermoso et al., 2012; Trecalli et al., 2012). Black shales are the hallmark of OAEs, and carbon isotope excursions are used to define their duration (Suan et al., 2008; Boulila et al., 2014; Burgess et al., 2015). Though the same OAE-defining isotopic excursions of black shales have also been recognized in platformal deposits (e.g. Weissert et al., 1998; Bodin et al., 2010, 2016; Trecalli et al., 2012; Phelps et al., 2014, 2015; Krencker et al., 2015), the contemporaneous shallow-water record of these events and their associated environmental stresses are more subtle and less well documented. Nevertheless, the sensitivity of neritic carbonates to changes in atmospheric and oceanographic conditions renders carbonate platforms highly detailed archives of these past environmental perturbations. Given that biochemical precipitation accounts for a large portion of Phanerozoic carbonate factories (Schlager, 2003), perturbations to the ocean-atmosphere system with which the biochemical precipitates equilibrate have the propensity to cause a carbonate factory demise or reorganization. In turn, carbonate platform architecture may be affected (e.g. Woodfine et al., 2008; Trecalli et al., 2012; De Keyser & Kendall, 2014; Phelps et al., 2014, 2015; Vahrenkamp et al., 2015; Preto et al., 2017).

The relationship between sedimentological and geochemical responses to OAEs in basin versus platform settings is relatively underexplored. Nevertheless, being able to recognize the sedimentological and geochemical signals of OAEs in shallow-water

carbonates could be a powerful tool in correlating basinal black shales to their neritic equivalents. This study focuses on characterizing the record of the Toarcian OAE in shallow-water carbonates of the Adriatic Carbonate Platform and addresses three problems; 1) what is the sedimentological and geochemical expression of the Toarcian OAE in shallow-water carbonates of the Adriatic Carbonate Platform, 2) how are these records manifested in different depositional settings, and 3) how did the Toarcian OAE affect platform architecture?

REGIONAL GEOLOGY

The southern Mediterranean carbonate platform that crops out along the east coast of the Adriatic Sea (Fig. 1) has been assigned several names in the past (Friuli, Dinaric, Istria, Adriatic) based largely on the region of study, and whether these deposits represent a laterally continuous or fragmented platform (i.e. an archipelago) (e.g. Korbar, 2009). More recently, however, Vlahović et al. (2002, 2005) proposed the use of the more unifying moniker, the Adriatic Carbonate Platform, to describe the contiguous, but morphologically variable, shallow-marine carbonate platform. Henceforth, we use this name to refer to the Lower Jurassic shallow-water carbonates outcropping along the eastern Adriatic region and their offshore equivalents in the Adriatic Sea (Fig. 1).

TECTONIC AND BASIN SETTING

Rifting of the northern margin of Gondwana that began in the Early Triassic resulted in the separation of the Adriatic (Apulian) plate from the African plate. An extensive epeiric platform developed during the initial phase of crustal thinning and subsidence, giving way to a huge, isolated carbonate platform in the southern Tethys as continental breakup ensued in the Middle Triassic (Vlahović et al., 2005). Thick evaporite deposition accompanied the initial stages of rifting in the Lower-Middle Triassic (Wrigley et al., 2015). Further rifting and disaggregation along deep-seated normal faults in the Lower Jurassic gave rise to several prominent isolated platforms including the well-studied Trento, Apulian, Campania-Lucania, and Apenninic platforms of Italy (e.g. Winterer & Bosellini, 1981; Woodfine et al., 2008). Late Pliensbachian disintegration, in particular, led to the connection of the Belluno and Ionian basins and thus the development of the Adriatic Carbonate Platform that crops out in NE Italy, Slovenia, Croatia, Bosnia and Herzegovina, Serbia, and Montenegro (Vlahović et al.,

2005) (Fig. 1). These platforms experienced shallow to deep-water sedimentation as they were variably and intermittently drowned during their pre-orogenic history.

North/south oriented grabens separating the isolated platforms were the site of deeper water pelagic and gravity-driven sedimentation from the platform margins (e.g. Belluno Basin: Bosellini et al., 1981; Lombardian Basin: Trecalli et al., 2012) (Fig. 2). The Adriatic Carbonate Platform emerged as one of the largest carbonate entities in the perimediterranean region of the Lower Jurassic (Vlahović et al., 2005). The same tectonic disintegration that saw the emergence of the Adriatic Platform formed the Adriatic Basin to the southeast, connecting the Ionian Basin of Greece and the Umbria-Marche and Belluno pelagic basins of Italy (Vlahović et al., 2005). The Slovenian-Bosnian Basin and Julian High bordered the Adriatic Carbonate Platform to the north (Fig. 2). Shallow-water carbonate sedimentation continued on the Adriatic Carbonate Platform until the Eocene when portions were incorporated into the External Dinarides via backthrusting during the Alpine Orogeny (Korbar, 2009; Placer et al., 2010). The study location encompasses Lower Jurassic platform carbonates of the Trnovki Gozd karst plateau and Bukovje area of western and south-central Slovenia, respectively (Fig. 1). These sites are structurally part of the Trnovo nappe situated at the farthest northwest extent of the External Dinarides (Placer et al., 2010). Palinspastic restoration of the study localities from Placer et al. (2010) are included in Figure 1.

LOWER JURASSIC STRATIGRAPHY OF THE ADRIATIC REGION

Jurassic strata of the Adriatic Carbonate Platform overlie the Upper Triassic Main Dolomite (Dachstein), a lithostratigraphic unit common to the European Alps that is composed of lagoonal-peritidal "lofer cycles" in the Adriatic region (Fischer, 1964; Goldhammer et al., 1990; Vlahović et al., 2005; Čadjenović et al., 2008; Sabatino et al.,

2013). The Lower Jurassic (Lias or Liassic) of Slovenia has been previously subdivided into 3 main lithostratigraphic units: 1) grain-rich bituminous dolomite of the Lower Liassic, 2) lithiotid limestones and dolomite of the Middle Liassic, and 3) spotted limestones of the Upper Liassic (Dozet, 1997). This subdivision is broadly correlatable throughout Croatia, Bosnia and Herzegovina, and Montenegro (Sabatino et al., 2013; Tišljar et al., 2002). The litho- and biostratigraphy of the Adriatic Carbonate Platform follows the seminal work done in the Southern Appenines (Sartoni & Crescenti, 1962; De Castro, 1962, 1963), with formal correlations to the External Dinarides revealing equivalent Lower Jurassic successions (Farinacci & Radoičić, 1964).

Lower Jurassic shallow subtidal shelf carbonates of Slovenia that belong to the Adriatic Carbonate Platform are subdivided into 2 cenozones (i.e. stratigraphic levels characterized by specific microfossil associations; Sartoni & Crescenti, 1962): the Lower Liassic – Middle Liassic cenozone is named after the characteristic green algal species, *Palaeodasycladus mediterraneus* (Dozet, 1997). The Upper Liassic cenozone of southwest Slovenia and Croatia is not defined by any characteristic fauna, but rather by a distinct spotted appearance, warranting designation as the "spotted limestones."

Palaeodasycladus mediterraneus Cenozone

In southeast Slovenia, the *Palaeodasycladus mediterraneus* cenozone contains an abundance of the Lower Jurassic bivalves known as lithiotids, including the species *Lithiotis problematica* and *Cochlearites loppianus*, as well as the lituolid benthic foraminifera *Orbitopsella primaeva* and *Orbitopsella praecursor* (Dozet, 1997). *Palaeodasycladus mediterraneus, Orbitopsella primaeva,* and *Orbitopsella praecursor* have a Hettangian-Pliensbachian range in the Karst Dinarides (Septfontaine et al, 1991; Sabatino et al., 2013; Gale, 2014), and are thus used as Pliensbachian index fossils in this

study. The "Lithiotid Limestone" of the Trnovski Gozd study area (Črne & Goričan, 2008) belongs to the *Palaeodasycladus mediterraneus* cenozone and encompasses shallowing upward peritidal cycles at its base that are overlain by moderate to high energy oncoid-peloidal grainstones and packstones. Though true lithiotid species are rare to nonexistent in the outcrops of Trnovski Gozd, the presence of the bivalve species *?Lithiopedalion* and *Gervilleioperna* (Črne & Goričan, 2008) that are commonly associated with lithiotids in other Lower Jurassic outcrops of the Dinarides, have led previous workers to lump these deposits with the lithiotid limestone lithostratigraphic unit that is correlatable across the most of the Adriatic Carbonate Platform (Črne & Goričan, 2008). Typical lithiotid limestones reflect a shallow subtidal shelf environment.

Spotted Limestone Cenozone

Spotted limestone lithofacies commonly overlie Lithiotid limestones of the *Paleodasycladus mediterraneus* cenozone in Slovenia and Croatia (Dozet, 1997, 2009; Vlahović et al., 2005; Sabatino et al., 2013) and have been associated with the early Toarcian drowning and the onset of the early Toarcian OAE (Črne & Goričan, 2008; Sabatino et al., 2013). The spotted limestones, or Fleckenkalk, as termed by 19th century Austrian Alps workers, have previously been attributed to extensive soft sediment bioturbation and late dolomitization and iron oxide weathering concentrated along burrows (Dozet, 1997; Sabatino et al., 2013). In southeast Slovenia this unit contains few calcareous algae, platycopid ostracods, and small gastropods, suggesting a restricted shelf environment (Dozet, 1997).

At Gornje Jelenje, in Croatia (Fig. 1), the spotted limestones contain calcareous mudstones and pelletal wackestones, with skeletal wackestone/packstone interbeds containing bivalves, peloids, ostracods, pelagic crinoids, benthic foraminifera, discrete

ooid horizons, and centripetally micritized cortoids of the aforementioned grains (Sabatino et al., 2013). Skeletal diversity and abundance are markedly less than the typical shallow subtidal- to intertidal skeletal facies of the *Palaeodasycladus mediterraneus* cenozone (Tišljar et al., 2002; Sabatino et al., 2013). *Thalassinoides* is the only recognizeable ichnogenus within the spotted limestones of Croatia (Sabatino et al., 2013). Few sedimentary structures are preserved due to the bioturbation and weathering pattern; however, possible hummocky cross-stratified intervals have been documented in Croatia (Sabatino et al., 2013), suggesting deposition in water depths greater than 10 m (Dumas & Arnott, 2006; Snedden et al., 1988).

METHODS

Lower Jurassic outcrops of the Trnovski Gozd and Bukovje areas (Fig. 1) in Slovenia were studied for sedimentological, paleontological, and geochemical purposes. Two stratigraphic sections were produced near the villages of Kovk and Gozd in the Trnovski Gozd area, as well as a third section from the Bukovje area (Fig. 1). Hockey puck sized samples were collected at 0.1 to 5 m vertical spacing at each location for further laboratory analyses.

STRATIGRAPHIC LOGGING AND SAMPLING

Stratigraphic sections Kovk and Gozd were logged and described using the modified Dunham Classification of Embry & Klovan (1971). Initial sampling for petrography was done approximately bed-by-bed roughly every 0.5-3 m at both Gozd and Kovk, yielding 40, and 35 samples, respectively. With age constraints of the Kovk and Gozd sections provided by index fossil identification in thin section, a second round of sampling was conducted for geochemical analyses. The Kovk section provided the most complete section of Pliensbachian through Toarcian strata and was thus chosen for higher resolution chemostratigraphy. Where outcrop quality permitted, approximately 0.25 meter resolution sampling was achieved within the suspected OAE interval at Kovk, while approximately 0.5-1.0 m resolution sampling was done throughout the rest of the section, yielding 63 samples total. Lower Jurassic outcrops of the Bukovje area of southwest Slovenia are heavily vegetated and tilted 30-35°, preventing detailed sub meter-scale stratigraphic logging that was achieved at Kovk and Gozd. A section was thus measured by differentiating major lithostratigraphic units per the biozanation of the region. Representative samples of each major facies at Bukovje were collected for petrographic and elemental analyses.

PETROGRAPHY

Thin sections from Kovk, Gozd, and Bukovje were analyzed using standard transmitted light microscopy in plane and cross polarized light at the University of Texas at Austin and at Institute of Palaeontology ZRC SAZU, Ljubljana. Half of each section was stained with alizarin red-S and potassium ferricyanide to discern dolomite, and ferroan carbonate (Dickson, 1966). Two hundred random points were counted from full section images of thirty-five 2 x 4.5 cm thin sections from the Kovk section using JMicrovision software. In order to statistically characterize the grain composition of each sample, two hundred randomly selected grains (i.e. every component but cement, mud, and porosity) were counted. 200 random skeletal grains were also counted to understand the skeletal makeup of each sample. Statistical uncertainty in the grain composition determined using this method is estimated to be approximately 6% (van der Plas & Tobi, 1965).

GEOCHEMISTRY

Scanning Electron Microscopy

Scanning electron microscopy (SEM) of select thin sections was conducted using a JEOL JSM-IT100 LA scanning electron microscope at the Institute of Palaeontology ZRC SAZU, Ljubljana. Roughly polished thin sections were mounted with double-adhesive carbon tape on 75 mm diameter aluminum holders. Uncoated thin sections were observed and photographed in low-vacuum mode (40 Pa) with an accelerating voltage of 15 kV and 20 kV at a working distance from 9 to 11 mm. Photomicrographs were taken in shadow backscattered electron imaging mode. Selected thin sections were carbon coated using a JEOL JEC-530 Carbon Coater and observed and analysed in high vacuum mode.

Energy-dispersive X-Ray Spectroscopy

Energy-dispersive X-ray spectroscopy (EDS) analyses were performed at the same low-vacuum (LV) conditions. Elemental spectra were obtained on uncoated specimens using point or small area analysis with 100 seconds pre-set (live) time and automatic element identification mode. Elements selected from qualitative results were further analyzed manually in (semi) quantitative (standardless) mode; results were calculated and reported in pure (non-oxide) form. EDS elemental mapping was performed at pre-set probe current and process time parameters, at a count rate of >20.000 counts per second.

X-Ray Fluorescence

Elemental abundances were determined at the Bureau of Economic Geology, Austin, Texas, from hand samples that were carefully cut and screened for weathered surfaces, fractures, stylolites, and veins. Major elemental concentrations were acquired using a Bruker handheld T3S X-ray fluorescence gun with a DeWitt Systsems Helium Purge unit. A rhodium source tube was used and set at 15 kv with an upper detection limit of 23 uA. Trace elemental abundances were determined using a Bruker handheld T4S x-ray fluorescence gun. The rhodium source tube was set at 40 kv with an upper detection limit of 19 uA. Quality assurance and control for real time results was ensured using the method and reference standards described by Rowe et al. (2012).

Mercury Concentration Measurements

Samples were screened for fractures/veins, stylolites, and weathered surfaces then carefully ground to a fine homogenized powder using an agate mortar and pestle and a Ring & Puck mill Shatterbox. Total mercury was measured using a Hydra II_c Direct Mercury Analyzer (Teledyne Leeman Labs) at Dickinson College. Quality assurance and

control for real time results was ensured by generating 10% analyses of certified and in-house reference standards, random duplicates, and blanks. Reference standards included NIST 1575A (certified) ([Hg] = 39.9 ppb) and NIST 1646A (in-house) (mean [Hg] = 29.6 ppb).

Organic Carbon Measurements

Samples were powdered and homogenized using an agate mortar and pestle and a Ring & Puck mill Shatterbox. They were then acidified with 1 M hydrochloric acid in 50 mL polypropylene centrifuge tubes so as to remove all carbonate. Centrifuge tubes were placed in a sonic bath heated to 70°C under a fume hood to expedite the reaction. Samples were centrifuged to separate the neutralized liquid from the residual material, and the supernatant liquid was decanted. The process was repeated 2-3 times until the remaining solid no longer reacted with the acid while sonicating. Approximately 15 mL of acid was added to the residual material and the mixture was left in a drying oven overnight at 70°C to react any remaining carbonate. Samples were then washed twice with deionized water following the same centrifuge and decanting method. Residual material was carefully collected by adding deionized water to the centrifuge tubes and filtering the mixture through glass fiber filters within glass filter tubes connected to a standard filtration vacuum pump system. The glass fibre filters containing the residual material were packed into tin capsules and dried overnight at 70°C. $d^{13}C$ and total organic carbon were analyzed using a Costech elemental analyzer (EA) with a Costech zero-blank autosampler that is coupled to a Thermo Electron Delta V continuous flow isotope ratio mass spectrometer at the University of Texas at Austin. Quality control was monitored by generating 10% analyses of certified reference standards and blanks. Quality assurance for the sample acidification and preparation method was ensured by

decarbonating 2 aliquots of the same sample and analyzing them separately. 10% or less difference between analyses of the same sample were produced for several samples. Results for reference standards and duplicates can be found in the supplemental material. A carbon isotope calibration curve was generated using analyses of the internally distributed standards USGS24 ($d^{13}C$ = -16.05 VPDB), IAEA-C5 ($d^{13}C$ = -25.49 VPDB), and IAEA C-7 ($d^{13}C$ = -14.48 VPDB). Total organic carbon (TOC) is calculated using a calibration curve obtained from measured peak areas of NIST SRM 8704 (i.e., Buffalo River Sediment) with a total carbon = 3.351%.

Bulk Carbonate Carbon and Oxygen Measurements

Approximately 0.3 mg aliquots of the same powdered samples prepared for organic carbon analyses were analyzed for the $d^{13}C$ and $d^{18}O$ of the bulk carbonate using a ThermoFisher Scientific GasBench II coupled to a ThermoFisher Scientific MAT 253 Isotope Ratio Mass Spectrometer at the University of Texas at Austin. Aliquots were reacted with 103% anhydrous phosphoric acid at 50°C for 2 hours. The majority of samples contained pure calcite; however, 4 samples contained mixed dolomite/calcite as determined petrographically and by the Mg/Ca ratio of the bulk XRF results. The reaction time and temperature were thus deliberately chosen to ensure that the carbon dioxide (CO_2) analyzed from the acidification reaction was largely a product of the dissolution of calcite, as opposed to dolomite, which reacts with H_3PO_4 at approximately 70°C (Ettinger et al., 2017). Data are calibrated using calcite standards NBS-18 ($d^{18}O$ = -23.0‰ VPDB, $d^{13}C$ = -5.0‰ VPDB) and NBS-19 ($d^{18}O$ = -2.3‰ VPDB, $d^{13}C$ = 1.95‰ VPDB).

RESULTS

SEDIMENTOLOGY OF TRNOVSKI GOZD

The Kovk and Gozd measured sections of this study are displayed in Figure 3. Grain distribution and skeletal composition diagrams derived from point counting are displayed beside the Kovk section (Fig. 3). A Pliensbachian-aged coral patch reef and lithiotid biostrome occur approximately 15 m from the base of the Gozd section (Turnšek et al., 2003). Shallow water carbonates with the typical *Palaeodasycladus mediterraneus* microfacies make up the first Gozd unit (Fig. 4A). Lithiotid-involutinid foraminifera-peloidal packstones to floatstones (Fig. 4C) make up the base of the section, whereas the equivalent strata of Kovk include the same facies plus an abundance of oncoidal-peloidal packstones to grainstones (Fig. 4B), and *Palaeodasycladus mediterraneus* float- to rudstones. *Palaeodasycladus* float- to rudstones are typically associated with a muddier foraminiferal-peloidal wackestone to packstone matrix. Planar tabular cross-stratified, superficial ooid-peloidal packstones and grainstones (Fig. 4D) occur throughout the oncoidal facies.

Rippled oolitic-encrinitic sands at Kovk overlie the oncoid-rich section and correlate to a planar tabular stratified ooid-crinoidal grainstone at Gozd (Fig. 3). The facies transition marks the last appearance of the Pliensbachian foraminifera index genus, *Orbitopsella*. The rippled oolitic-encrinitic grainstones of Kovk are abruptly overlain by a prominent ferruginous hardground level (Fig. 3) that contains a condensed and amalgamated succession of hardgrounds (Fig. 5A) and discrete, centimeter-scale, brachiopod-oolitic-crinoidal packstone beds (Figs. 5B, 5C). *Bacinella* and *Girvanella* oncoids also occur within the hardground interval. The mud-rich matrix contains abundant glauconite (Figs. 5A, 5C), micron to millimeter-scale, oxidized pyrite pellets (Fig. 5B), horizons densely populated by terebratulid brachiopods (*?Soaresirhynchia*

bouchardi) (Fig. 5D), calcispheres (Fig. 5E), thin-shelled molluscs (Fig. 5E), Nodosariid foraminifera, disarticulated vertebrate material (Figs. 5F, 5G). The hardgrounds also notably contains dissolution surfaces (Fig. 5B) and uncompacted *Chondrites* burrows. At Gozd, the succession underlying the hardground interval is similar to Kovk, but is truncated short of the hardground interval by a normal fault that removed an indeterminate amount of stratigraphy (Fig. 3).

At Kovk, approximately 15 m of crinoidal-ooid packstones to grainstones overlie the hardground interval (Fig. 3) and contain accessory brachiopods, cortoids, and rare miliolid foraminifera towards the top of the unit. Planar tabular cross stratification as well as grain-to-grain compaction and spalling within ooids are common (Fig 6A). A prominent, nodular-bedded interval overlies the crinoidal-ooid grainstone unit (Fig. 3) and is composed predominantly of sponge boundstones and skeletal wackestones with brachiopods, juvenile ammonites, and abundant serpulid worm tubes (Fig. 6C). The nodular-bedded sponge-rich interval is correlatable to the same facies between 30-33.5 m at Gozd, where it overlies compacted skeletal-oolitic packstones and grainstones (Fig. 3). The nodular sponge-rich interval at Gozd and the underlying grainstones directly overlie fault gouge breccias, and have been restored to their approximate original stratigraphic position by hanging them on the height of the base of the nodular-bedded interval at Kovk (Fig. 3).

Moderately to well-sorted, crinoidal-ooid grainstones (Fig. 6E) overlie the nodular, sponge-rich interval at both Kovk and Gozd, and mark the top of the Gozd section. Ooids display well-developed acicular isopachous cements and are uncompacted (Fig 6D). At Kovk they grade upward into intraclastic-brachiopod-crinoid-ooid grainstones and packstones before abruptly transitioning into a *glossifungites*-burrowed wackestone with a scalloped erosional top surface (Fig. 3). Skeletal-oolitic grainstones

directly overlie and infill the burrows of the hardground horizon and mark the top of the Kovk section.

SEDIMENTOLOGY OF BUKOVJE

Three distinct units were recognized at Bukovje. An approximately 50 m interval containing the typical lithiotid limestone of the *Palaeodasycladus mediterraneus* cenozone characterizes the lower unit. The second unit is approximately 67 m thick and also contains fauna of the *Palaeodasycladus mediterraneus* cenozone, but is distinguished from the underlying unit by an abundance of ooids. It is capped by peloidal packstones and fenestral laminites. The third unit is 50+ m thick and composed of the spotted limestones that are widely distributed across southeastern Slovenia and Croatia. The spotted limestones are variably organic-rich and display muddy *Planolites*-burrowed wackestones to packstones (Fig. 7A), skeletal-oolitic grainflows (i.e. discrete <5 cm grain-rich structureless deposits) overlying organic-rich mudstones at erosive contacts (Fig. 7B), lithoclastic breccias in which the clasts are organic-rich mudstones (Fig. 7C), and less organic-rich, massively bedded mudstones (Fig. 7D). Organic-rich intervals with oxidized pyrite framboids account for the spotted appearance at Bukovje (Fig. 7D-G).

STABLE ISOTOPES

Marine Organic Matter

Carbon isotope ratios for occluded marine organic matter of samples from the Kovk section are shown in Table 1, and Figures 3 and 7. Isotopic values show a 1.6‰ negative trend from the base of the section to approximately 6 m, where the values fluctuate between approximately -27 and -28‰ for a further 5 m. Between approximately 11-12 m, the profile takes a 1.2‰ positive trend coincident with the appearance of the ferruginous hardground interval. This trend is interrupted by a sharp 2.2‰ negative

carbon isotope excursion coincident within the ferruginous hardground. Over a 2 m interval within the ferruginous hardground interval, values increase by 3.2‰ in a positive linear trend before dropping by approximately 2.0‰ to -27.7‰ at the top of the hardground interval.

Between 16-30 m values fluctuate between approximately -27.8 and -26.6‰ with a mean value of -27.31‰. A -1.02‰ trend defines a second negative carbon isotope excursion coincident with the appearance of the sponge-rich nodular limestone between 31.3-33.9 m. A broad positive trend in the carbon-isotope values follows this second excursion between 33.9-44.8 m.

Bulk Carbonate

Carbon isotope ratios for bulk carbonate samples from the Kovk section are shown in Table 1 and Figures 3 and 8A. A negative excursion of 1.1‰ is recognized below the first organic carbon negative negative carbon isotope excursion between 3.3-10.4 m. Throughout the interval encompassing the first negative negative carbon isotope excursion in the organic carbon values and the underlying positive trend (11-13.2 m), bulk carbonate values show little fluctuation. A 1.21‰ positive trend in the bulk carbonate values between 13.18-15.38 m, however, mirrors the positive linear trend in organic carbon values above the first organic negative negative carbon isotope excursion (Figs. 3, 8A). Bulk carbonate values drop again to 2.12‰ at 16.4 m and increase linearly over the next 15 m to 3.13‰. Minor fluctuations in the bulk carbonate values occur upward throughout the remainder of the section, ranging from 2.15 to 2.83‰.

Oxygen isotope ratios for bulk carbonate samples from the Kovk section are listed in Table 1 and Figure 8A. From 0-5 m, $\delta^{18}O$ values range between -0.33 to -0.72‰, with an average value of -0.56‰. Between 5-15.5 m values fluctuate between -0.49 to -

1.99‰, with an average value of -1.05‰. From 16.3-30.5 m, values increase from -1.83 to -0.29‰ in a positive linear trend. Thereafter they fluctuate between -0.22 to -1.41‰ with an average value of -0.66‰.

ELEMENTAL CONCENTRATIONS

Pertinent major and trace element concentrations for the Kovk section discussed in this paper are displayed in Table 2 and Figure 8. Additional elemental abundances determined via the handheld XRF method that are not further discussed in this paper can be found in the supplemental material. Hg, V, Ni, and Mo are normalized to Al and/or TOC, where data permitted, to account for their affinity for detrital and organic-rich sediments, respectively (Fig. 8B). Background Al concentrations fall between 0-0.2% throughout the majority of the section with elevated values of between 0.2-1.0% at 4 m, 12-14.5 m and 30 m. Background Ti concentrations are less than approximately 0.02%, with enrichment between 0.02-0.06% at 12.2-14.5 m and 29.6 m. Background Hg concentrations are approximately less than 2 ppb with enrichment as high as 10.3 ppb at 12.2-23.9 m, 35.5 m, 41.1 m, and 46.4-48.0 m. Background Fe concentrations are less than 0.3%, with enrichment as high as 0.6% at 4 m, between 12.2-16.3 m, and 28.8-29.6 m. Background Mn concentrations are approximately 185-190 ppm with depletions as low as 178 ppm occurring at 12.2-14.5 m, 21.5 m, and 27.8-29.6 m. Background concentrations of trace elements V, Ni, and Mo are approximately 80 ppm, 10 ppm, and 1 ppm, respectively. TOC values are variable, with a range of 0.002-0.02%. Background concentrations of Ba and P are approximately 100 ppm and 0.015%, respectively.

INTERPRETATION

FACIES ASSOCIATIONS

The facies associations of Trnovksi Gozd are labeled adjacent to the depth column of each section in Figure 3, along with the interpreted transgressive/regressive cycles. Facies associations are subdivided by typical flat-topped platform (Read, 1985) versus carbonate ramp (Kerans & Fitchen, 1995) facies associations (1 and 2, respectively). Facies association 1a is interpreted to be a low energy, shallow subtidal to lagoonal environment. Lithiotid-dasyclad rudstones (Fig. 4A) are indicative of a shallow subtidal, open circulation, protected setting or lagoon, similar to modern day dasycladacean meadows (Elliott, 1968, 1991). Facies association 1b includes diverse skeletal packstones and oncoid floatstones (Fig. 4B) reflecting a low to moderate energy, shallow subtidal, open circulation environment. Oncoids are formed primarily by *Thaumatoporella*, *Girvanella*, and *Bacinella* encrustations with a variety of skeletal and peloidal nuclei. Irregular forms are attributed to lower energy, shallow subtidal settings and are limited to packstones, while rounded oncoids are found in both packstones and grainstones and likely formed in more open marine, energetic settings. Facies association 1c includes the peloidal-crinoid-superficial ooid grain-dominated packstones and grainstones, and reflects a shallow subtidal, moderate to high-energy environment (Fig. 4D). The energy shadow for quiet water oncoid growth and the development of dasycladacean meadows may have been provided by any combination of these peloidal-oolitic grainstone shoals, coral patch reefs, and modest lithiotid buildups (c.f. Posenato & Masetti, 2012).

Facies association 1d encompasses the ferruginous hardground interval and represents a condensed section with low sediment accumulation rates, as evidenced by the abundance of glauconite (Figs. 5A, 5C) and uncompacted burrows. Highly abraided grains within the rare packstone intervals suggest infrequent storm transport (Fig. 5C),

while low diversity, intact terebratulid communities (Fig. 5D), and dark-colored, organic-rich sections with calcispheres (Fig. 5E) likely reflect periods of quiescence. The presence and preservation of pelagic fauna (calcispheres, juvenile ammonites, ostracodes, phosphatic vertebrate material) suggest deposition in water much deeper than the underlying facies associations. We thus interpret facies association 1d to reflect water depths between fair weather and storm weather wave base in an environment transitional between a drowned flat-topped carbonate platform (c.f. Schlager, 1981, 1989) and a distal outer ramp environment (Kerans & Fitchen, 1995). Facies association 2a includes low angle cross-stratified crinoidal-ooid grainstones (Fig. 6E) and skeletal-oolitic packstones. Ooids are radial and well preserved, and the fabric of the oolites completely lacks any oomoldic porosity, suggesting they were likely originally calcitic. A lack of marine isopachous cements that are otherwise expected in grains washed around in wave-modulated settings suggests that these were deposited in a lower energy, subtidal setting. Partial micritization and compaction of the ooids (Figs. 6A, 6C), in particular, point to the transport of these grains from the actual carbonate factory from whence they formed. Abundant intraclasts occur in the uppermost grainstone of the thick facies association 2a accumulation (Fig. 3) and moderate to poor sorting of ooids throughout the different grainstones further suggests energetic and episodic storm transport. Given this evidence and by applying a Waltherian prediction of upward facies transitions from the distal outer ramp hardground underlying the main 2c accumulation, we interpret facies association 2a to reflect a proximal outer ramp setting, slightly below fair weather wave base. Grain-rich accumulations are likely the product of grains being swept from more proximal to distal areas along a ramp profile.

Facies association 2b includes the nodular-bedded, sponge-rich wackestone and *Glossifungites*-burrowed wackestone towards the top of the Kovk section (Fig. 3).

Uncompacted burrows (Fig. 6C) and classic *Glossifungites* within these units suggest early marine cementation and hardground formation. Sediment starvation leading to hardground formation and the appearance of articulated pelagic fauna such as juvenile ammonites (Fig. 6B) and calcispheres indicate deeper water deposition. We interpret facies association 2b to reflect an outer ramp environment. Facies association 2c includes low angle, cross-stratified crinoidal-ooid grainstones, clean ooid grainstones, and stratified ooid-intraclastic grainstones. Ooid grainstones are well sorted and have well developed acicular isopachous cements (Fig. 6F). This, along with the resultant lack of compaction, suggests deposition in shallow, constantly agitated water. We thus interpret facies association 2c to reflect the ramp crest environment.

Lithostratigraphic Age Constraints

The lack of biostratigraphically relevant ammonites in Lower Jurassic sediments of Trnovski Gozd complicates the age interpretation. On a coarse scale, however, typical *Palaeodasycladus mediterraneus* microfacies are characteristic of the Pliensbachian biozone. Of particular importance is the last appearance of the benthic foraminifera *Orbitopsella* (Fig. 3), which has been ascribed a Domerian (upper substage of the Pliensbachian) maximum age (Septfontaine et al., 1991). Spotted limestones of the Adriatic region have been associated with the Toarcian stage (Dozet, 1997; Sabatino et al., 2013; Tišljar et al., 2002), and are similarly used to identify the Toarcian stage in the Bukovje outcrops of this study. Though Trnovski Gozd lacks diagnostic spotted limestones, Črne & Goričan (2008) correlated the ferruginous hardground interval of Kovk to the spotted limestones of Southwest Slovenia. Furthermore, the authors attributed the appearance of the ferruginous hardground of Trnovski Gozd to the onset of the 2nd order transgression in the NW Tethys (Hardenbol et al., 1998), which corresponds

to a global eustatic sea-level rise (Hallam, 1981). Within, and just above the hardground interval, calcispheres and other pelagic fauna support a relative deepening broadly consistent with the early Toarcian transgression, and glauconitic accumulations and hardground formation suggest partial drowning. We therefore interpret the ferruginous hardground interval (facies association 1d) to be early Toarcian in age, and the last appearance of *Orbitopsella* to mark the late Pliensbachian (Fig. 3).

GEOCHEMICAL RECORD

Carbon Isotopes

Between approximately 11-15 m, the organic carbon isotope profile for Kovk displays the same positive-negative-positive trend (Figs. 3, 8) characteristic of early Toarcian sections from the Croatian part of Adriatic Carbonate Platform (Sabatino et al., 2013) (Fig. 1). The sharp negative negative carbon isotope excursion bounded above and below by two positive trends is characteristic of global carbon isotope profiles of the early Toarcian (Jenkyns & Clayton, 1997; Hesselbo et al., 2007; Bodin et al., 2010; Gröcke et al., 2011; Sabatino et al., 2013), and demarcates the early Toarcian OAE. The underlying values do not show an obvious preceding negative negative carbon isotope excursion that might demarcate the Pliensbachian-Toarcian event; however, the bulk carbonate isotopic record between 3.3-10.1 m displays a more obvious stepped negative trend of about 1.1‰ maximum magnitude between the base and top of the excursion. The equivalent interval in the organic carbon isotopic record also displays an overall negative trend, with values fluctuating between -28.0 and -26.9‰ throughout the main negative deflection between (4.0-10.4 m). The top of this overall negative trend in the organic carbon isotopic values and the top of the bulk carbonate negative negative carbon isotope excursion correlate to the last appearance of the Pliensbachian index genus, *Orbitopsella*

(Fig. 3). As such, we interpret this interval underlying the main early Toarcian OAE to be the Pliensbachian-Toarcian event.

Though the positive trend preceding the negative negative carbon isotope excursion that demarcates the early Toarcian OAE in the organic carbon record and the OAE excursion itself are not recorded in the bulk carbonate record, the broad positive trend following the maximum negative excursion within the OAE is faithfully recorded in the bulk carbonate values between 13.2-15.0 m (Figs. 3, 8). The bulk carbonate record also shows a negative negative carbon isotope excursion between 31.4-33.1 m coincident with the negative negative carbon isotope excursion in the organic carbon record.

Oxygen Isotopes

Bulk isotopic values, particularly $d^{18}O$ ratios, can be influenced by isotopic fractionation associated with biomineralization, the presence of non-marine cements, neomorphism of primary aragonite, and diagenetic re-equilibration (Dickson & Coleman, 1980; Brand & Veizer, 1981; Marshall, 1992). As such, it is presumable that the bulk oxygen isotopic values ascertained for the Kovk section do not reflect original marine values, but rather a diagenetic overprint on pre-existing marine values. Nevertheless, broader trends in the values are discernible, and may reflect vestiges of inherited isotopic composition of the primary skeletal and abiotic marine precipitates. In particular, from the base of the section to the top of the OAE, average $d^{18}O$ for both the Pliensbachian-Toarcian event and OAE intervals are 0.62‰ lighter than those preceding and between the events (Fig. 8A), suggesting that these intervals were warmer than the bounding periods of comparatively cooler temperatures (Grossman & Ku, 1986). This observation is consistent with the documentation of increased sea-surface and bottom water temperatures for both the Pliensbachian-Toarcian event and the early Toarcian OAE (e.g.

Suan et al., 2008; Krencker et al., 2015). Following the OAE, relatively negative $d^{18}O$ values increase linearly by approximately 3‰ towards 30.5 m, defining a possible cooling trend following the early Toarcian OAE (Fig. 8A). Thereafter, they fluctuate between -0.50 to -1.41‰ throughout the remainder of the section.

Mercury Distribution

The mercury concentration of marine sediments has recently been used as a proxy for large igneous province volcanism (Pyle & Mather, 2003; Sanei et al., 2012, 2013; Percival et al., 2015; Grasby et al., 2016; Thibodeau et al., 2016). In the case of the Pliensbachian-Toarcian event and the early Toarcian OAE, enrichments in mercury have been used to implicate the Karoo-Ferrar-Chon Aike province as the trigger for both biotic crises and the widespread deposition of organic carbon-rich black shales during the Toarcian OAE (Percival et al., 2015, 2016). Large volcanic episodes such as those in the late Pliensbachian and early Toarcian have the propensity to induce substantial increases in the concentration of atmospheric Hg. The relatively long atmospheric residence time of $Hg^0_{(g)}$ (~1 year, Pyle & Mather, 2003) enables large volcanic inputs of Hg to have a global distribution prior to incorporation into marine sediments. Globally distributed enrichments in Hg are thus a proxy for large igneous province activity. Note, however, that marine organic matter acts as a major sink for Hg, and must, therefore, be accounted for when trying to discern true volcanic signatures of Hg in marine sediments from fluxes in organic carbon burial.

Extremely low concentrations of mercury are present throughout the Kovk section (Table 2, Fig. 8A), as is expected for relatively shallow-water carbonates with low total organic carbon (TOC) burial. Nevertheless, subtle enrichments occur during the Pliensbachian-Toarcian Event (Fig. 8A). These enrichments become more prominent

after normalization to total organic carbon, particularly in the latter half of the event (Fig. 8A). A relatively large peak in the concentration of mercury within the ferruginous hardground closely follows the base of the abrupt negative negative carbon isotope excursion that demarcates the early Toarcian OAE (Fig. 8A). Mercury concentrations remain elevated throughout the OAE interval, with a maximum occurring just above the broad upper positive carbon isotope trend at the top of the OAE (Fig. 8A). Uncertainty in the values of samples that were run as duplicates are significantly less than the magnitude of the mercury enrichments within the Pliensbachian-Toarcian event and OAE intervals, indicating that these enrichments are not a result of noise inherent to the analytical or sampling methods. Furthermore, the enrichments throughout the Pliensbachian-Toarcian event and the OAE interval remain significant after normalization to TOC (Fig. 8A), suggesting that they are not simply noise in the distribution of mercury throughout the section. Hg enrichments coincident with the Pliensbachian-Toarcian event and the Toarcian OAE are not the result of enhanced organic carbon burial, but likely reflect pulses in activity of the Karoo-Ferrar-Chon Aike large igneous province. This is in agreement with the studies by Percival et al. (2015, 2016). Enrichments in Hg also occur after the OAE at Kovk, and are interpreted to reflect continued volcanism in the Karoo-Ferrar-Chon Aike Large Igneous Province.

Detrital Element Distribution

Detrital flux proxies such as aluminum and titanium can be used to infer relative weathering trends (Tribovillard et al., 2006; Zhang, et al., 2014), and are thus useful proxies for weathering in the Lower Jurassic, which saw elevated continental weathering during both the Pliensbachian-Toarcian event and the early Toarcian OAE (Bodin et al., 2010, 2016; Krencker et al., 2015; Montero-Serrano et al., 2015). However, as an isolated

carbonate platform, the Adriatic Carbonate Platform received no riverine continental input during the Lower Jurassic and thus has no siliciclastic component. This can be observed in the insignificant baseline concentrations of Al and Ti (Fig. 8A). Though tempting to relate increases in titanium and aluminum throughout the OAE (Fig. 8A) to elevated continental weathering, the isolation of the platform precludes the riverine input of siliciclastics. The concentration of Ti and Al throughout this interval is more likely related to other processes that may include glauconite accumulation (Figs. 5A, 5C) and aeolian input. Furthermore, extremely low sediment accumulation rates throughout the OAE are likely to exaggerate true weathering proxies.

Redox Sensitive Element Distribution

Under reducing conditions, the oxidation state of elements Fe, V, Ni, and Mo are lowered, and their incorporation into certain mineral phases (e.g. Fe and Mo into sulfide minerals), complexation onto surfaces, and incorporation into organics becomes thermodynamically favorable (Emerson & Huested, 1991; Lyons et al., 2009; Owens et al., 2016). These elements are preferentially incorporated into sediments overlain by waters depleted in oxygen, as well as within sediments containing anoxic pore waters. Enrichments in the trace elements V, Ni, and Mo coincide with the oncolitic facies of the Pliensbachian-Toarcian event, and the ferruginous hardground of the early Toarcian OAE (Fig. 8B); Fe is enriched (up to 6X) at the onset of, and throughout the OAE (Fig. 8B). TOC-normalized Mo and Ni values show enrichment within the Pliensbachian-Toarcian event and Mo is enriched at the onset of the lower positive organic carbon isotope excursion coincident with the stage boundary and appearance of the ferruginous hardground interval (Fig. 8B). The TOC-normalized enrichments indicate that elevations in redox sensitive elements are not just a result of oxygen-related facies variations within

these intervals, but rather a decrease in the dissolved oxygen levels causing these elements to precipitate. Furthermore, these data point to a significant interval of deoxygenation of the water column overlying the sediments in which these elements accumulated. Enrichments in redox sensitive elements during the OAE are either the result of oxygen-depletion in waters above the sediment-water interface, or within the shallowest several cm of the bottom sediment.

Framboidal pyrite formed during the OAE provides a more definitive indication of deoxygenation of the bottom water column at Bukovje (Fig. 7), and the presence of sub millimeter, rounded pyrite at Kovk (Figs. 5B, 5E) may also be the product of formation in the bottom water column (Wilkin et al., 1996; Jenkyns, 2010). Furthermore, micron-scale framboidal pyrite, Fe, and Mo enrichments are characteristic of euxinic conditions, where free hydrogen sulfide in the water column enables the precipitation of iron-sulfide minerals such as pyrite, within which Mo can be incorporated (Wilkin et al., 1996; Tribovillard et al., 2006; Gill et al., 2011; Jenkyns, 2010). Following enrichment in redox sensitive elements surrounding the Pliensbachian/Toarcian boundary and coincident with the lower positive excursion in the early Toarcian (11.4 m, see Fig. 8B), a broad drawdown in trace elements V, Ni, and Mo is recorded in the Kovk section throughout the OAE interval whilst Fe enrichment continues (Fig. 8B). In light of continued Fe enrichment and Mn depletion (Fig. 8B), as well as concomitant enrichments in redox-sensitive trace elements within organic-carbon rich shales of the adjacent basins (Fig. 10), we interpret the drawdown of redox sensitive trace elements to be the result of the sequestration of these elements in the adjacent basins and other anoxic basins around the NW Tethys, as opposed to a return to well-oxygenated conditions on the shelf. These interpretations are in close agreement with the depauperate skeletal assemblage and lack of carbonate production across the OAE.

Iron enrichment throughout the OAE is also supported by the ferroan calcite within primary marine precipitates (Fig. 5C). Brachiopods, crinoid fragments, and syntaxial cements within the OAE hardground interval at Kovk stained purple (Fig. 5C) in reaction with potassium ferricyanide, indicating the presence of ferrous iron (Dickson, 1966). It is not known whether the crinoids and their syntaxial cements were originally high-Mg calcite or low-Mg calcite, and thus is unclear whether they have been altered or not. However, low-Mg calcite terebratulid brachiopods are well-preserved, and thus record the incorporation of ferrous iron into their skeleton during their lifetime, as opposed to during post mortem diagenesis. The presence of ferroan calcite is a key indicator of reducing conditions, because under oxidizing conditions, Fe complexes with oxygen to form iron-oxyhydroxides preventing the incorporation of Fe into calcite, whereas under reducing conditions, Fe^{2+} can be readily incorporated into calcite (Evamy, 1969; Léonide et al., 2012). Prolonged deoxygenation thus occurred in either the bottom water, or the sediment pore water (up to several cm below the sediment-water interface) in which benthic organisms were living semi-infaunally and exchanging ions (Graziano et al., 2006).

Nutrient Sensitive Element Distribution

The early Toarcian OAE has been associated with pulses of increased continental weathering as a result of dramatic increases in atmospheric pCO_2 that led to increased global temperatures and an expedited hydrologic cycle (e.g. Percival et al., 2016). These pulses would have seen the increased delivery of essential biolimiting elements such as Ba and P to the oceans, resulting in surface water primary productivity spikes. The Kovk section records a subtle increase in Ba and sizeable increase in the amount of P at the onset of the OAE (Fig. 8B), indicating that deoxygenation of the shelf may have occurred

as a result of an increase in primary productivity and subsequent invasion of the oxygen minimum zone up onto the shelf. This interpretation is called into question, however, as enrichments in these elements may simply be the result of slow sediment accumulation (i.e. condensation) and the presence of minor amounts of disarticulated phosphatic bone remains within the hardground interval (Fig. 5F, 5G). Reducing conditions likely led to the preservation of these remains, and may have imparted P enrichment within the OAE interval. If considered a nutrient, and thus productivity proxy, the P enrichment substantiates previously interpreted productivity cycles and the expansion of the oxygen minimum zone documented in the adjacent Belluno Basin (Jenkyns et al., 1985; Bellanca et al., 1999) (Fig. 10). There, eutrophication and productivity cycles during the OAE were attributed to upwelling (Bellanca et al., 1999), but were likely augmented by the global increase in continental weathering coincident with pulses of volcanic activity (Percival et al., 2016). The presence of preserved bone marrow in the sediment (Fig. 5F, 5G), along with increases in nutrient element proxies (Fig. 8B), and redox sensitive element enrichment (Fig. 8B), suggest that an enhanced oxygen minimum zone expanded onto the carbonate shelf.

DISCUSSION

Numerous studies have focused on the documentation of bottom-water anoxia in basinal settings during OAEs by means of multiproxy geochemical and sedimentologic lines of evidence. Despite there being a critical link between sediment accumulation in basins and the production of sediment on adjacent platforms (or lack there of), comparatively few studies have been dedicated to the effect that OAEs have had on carbonate platforms that formed adjacent to many well-studied basins. The thickness of the OAE interval on the NW part of the Adriatic Carbonate Platform, based on the upper and lower bounds of the negative organic carbon isotope excursion, is 3.04 m at Kovk (Fig. 3). At Gornje Jelenje, Croatia, which represents the interior part of the platform, Sabatino et al. (2013) documented an approximately 35 m thick OAE interval. The disparity in thickness between the outer margin and interior of the platform requires significant growth on the platform interior (Fig. 9), which we interpret to be the result of the combination of differential subsidence (Fig. 9), and poor circulation on the platform interior. Subsidence may have been enhanced by halokinesis in underlying Triassic evaporites. Wrigley et al. (2015) interpreted major salt withdrawal related to foreland flexural rifting in the Late Jurassic from 2D seismic data of offshore Croatia. It is likely that halokinesis also influenced sedimentation in the Early Jurassic as a result of prevailing extensional tectonics and sedimentary loading. Differential subsidence on the platform interior further drove the disparity in circulation between the interior and platform margin, yielding greater accumulation within the intrashelf basin.

The duration of the early Toarcian OAE has been estimated from basinal sections via cyclostratigraphy anchored to radiometric dates. Tying the cyclostratigraphy to the upper and lower bounds of the negative carbon isotope excursion associated with the

OAE has produced duration estimates of 300 kyr to 900 kyr (Boulila et al., 2014; Suan et al., 2008, respectively). The carbonate accumulation rate during this interval on the Northwest part of the Adriatic Carbonate Platform (Kovk), not accounting for compaction or pressure dissolution, was thus between 3.4–10.1 m/Myr. By comparison, normal accumulation rates of pure carbonate platforms of the Jurassic are approximately 85 m/Myr (Bosscher & Schlager, 1993), indicating that the NW part of the Adriatic Carbonate Platform developed a significant discontinuity surface during the OAE (Fig. 9). This discontinuity is manifest in the ferruginous hardground interval (Fig. 3) and is further substantiated by glauconitic accumulations (Fig. 5A, 5C) in Kovk. Using the same parameters, the accumulation rate during the OAE within the inner part of the platform (Sabatino et al., 2013) was between 116-39 m/Myr. The median estimate for accumulation rates on the platform interior (77.5 m) is still less than the average carbonate accumulation rates for the Jurassic, but within the same order of magnitude. We interpret the differential accumulation on the margin versus interior to be the result of deepening of the platform interior, allowing for the deposition of fine-grained pelagic carbonate and organics in an intrashelf basin. The outer margin accumulated substantially less sediment throughout the OAE as a result of skeletal carbonate factory shutdown, combined with the still intermittently agitated water depths that precluded the preservation of pelagics.

Evidence for the restricted intrashelf basin can be found in the depauperate, organic-rich accumulations of the spotted limestone facies that are widely distributed across eastern Slovenia and Croatia (Fig. 7). Planolites burrows (Fig. 7A), sediment grain flow deposits with erosive bases (Fig. 7B), and abundant framboidal pyrite (Fig. 7D, 7E), along with previous reports of hummocky cross-stratification (Sabatino et al., 2013), support the establishment of mid-outer ramp setting in the platform interior. Furthermore,

the post-OAE Waltherian facies transitions at Kovk are consistent with typical ramp facies (Burchette & Wright ,1992; Kerans & Fitchen, 1995). The spotted appearance of the Toarcian section of Bukovje is attributed to oxidized pyrite framboids (Figs. 7F, 7G), and although not explicitly documented by Sabatino et al. (2013), the Gornje Jelenje site also has abundant sub-millimeter oxidized pyrite throughout the spotted limestone interval (Košir, pers. obs.). These observations suggest a euxinic regime in the intrashelf basin, which accounts for the preservation of organics. Furthermore, framboidal pyrite within the OAE black shales of the adjacent Belluno Basin (Bellanca, 1999) points to the development of euxinia in the basin as well. Anoxic to euxinic conditions on the platform were likely punctuated by the return to normal oxygenation, as evidenced by the proliferation of brachiopods and crinoids at discrete intervals within the OAE interval at Kovk (Figs. 5C, 5D), interbedded intervals of low-TOC facies at Bukovje (Fig. 7D), and burrowed intervals within the spotted limestones of Croatia (Vlahović et al., 2002; Tišljar et al., 2005; Sabatino et al., 2013). Pulses of oxygenation within dominantly anoxic to euxinic settings during the OAE have also been documented by Martindale and Aberhan (*in press*) in the Panthalassic Ocean. Following the OAE, carbonate production resumed around the platform margins, albeit by fundamentally different organisms and an abundance of radial ooids. In the platform interior, however, the spotted limestone facies was deposited throughout the remainder of the Toarcian (Fig. 9), indicating that deoxygenation likely persisted as a result of restricted circulation.

DRAWDOWN OF THE REDOX SENSITIVE ELEMENT INVENTORY

Trace Metals

Not all redox sensitive elements show depletions through the OAE interval; Fe is particularly enriched throughout the OAE, while trace elements Mo, Ni, and V are

depleted (Fig. 8B). Previous studies have proposed global drawdowns of redox sensitive trace element inventories during OAEs as a result of the increased sequestration of these elements during enhanced organic carbon burial (Algeo, 2004; Lyons et al., 2009, 2014; Jenkyns, 2010; Algeo & Rowe, 2012; Owens et al., 2016). This study provides unique insight into this phenomenon as a large depletion in the concentration of V during the OAE on the platform top is reciprocated by V enrichment in the OAE black shales of the adjacent Belluno Basin (Bellanca et al., 1999) (Fig. 10). The paucity of V and other redox sensitive trace elements during the OAE at Kovk further supports the scenario of a globally depleted seawater inventory of these trace metals. The mechanism for this depletion was likely the enhanced global organic carbon burial, which, due to the widespread reducing conditions, also sequestered large quantities of redox sensitive elements. The sequestration of these trace elements must have been substantial, as redox conditions remained favorable for their deposition on the shelf as evidenced by the continued enrichment of Fe throughout the OAE (Fig. 8B). Due to the scarcity of the trace elements Mo, Ni, and V in the oceans, the global drawdown in their inventory in seawater resulted in depletions of these metals in sediments of the Adriatic Carbonate Platform during the OAE. As Fe complexed out of seawater during the widespread reducing conditions of the OAE, the ocean Fe inventory may have been replenished by volcanic inputs and increased continental weathering. Fe^{2+} thus continued to be enriched under deoxygenated conditions as there was a comparatively abundant supply of it in the oceans, preventing any noticeable drawdown during the sequestration of it and other redox sensitive elements with global black shale deposition.

Manganese.--- Mn is an element with higher solubility in anoxic waters due to the fact that lower reduction potentials favor the aqueous phase of Mn^{2+} (Force & Cannon, 1988). Mn is thus an ideal proxy for paleoredox conditions, and has been

previously established as an especially sensitive marker for changes in paleoredox conditions during OAEs (Jenkyns, 2010; Lu et al., 2010; Sabatino et al., 2011). A caveat to this approach, however, is that Mn-rich carbonates can form in deoxygenated sediments that are rich in organics, because pore-water alkalinity is driven higher following organic-matter mineralization (Froelich et al., 1979; Burdige, 1993). With an ample supply of Mn^{2+}, significant diagenetic manganoan carbonate may precipitate in association with black shales. In the early Toarcian, the oceanic Mn flux was likely anomalously high as a result of hydrothermal input associated with increased seafloor spreading, yielding the ideal scenario for diagenetic Mn deposition in black shale successions (Corbin et al., 2000).

On the NW Adriatic Carbonate Platform, depletions in Mn occur in low-TOC carbonates at the onset of the Pliensbachian-Toarcian Event and throughout the Toarcian OAE at Kovk (Fig. 8B). These depletions correlate with enrichments in Fe, indicating that reducing conditions prevailed on the shelf at the onset of the Pliensbachian-Toarcian event and throughout the OAE. At Velebit A, Adriatic Carbonate Platform (Sabatino et al., 2013) and Monte Sorgenza, Campania–Lucania Carbonate Platform, Southern Italy (Lu et al., 2010), platform top carbonates also show Mn depletions through the negative negative carbon isotope excursion of the Toarcian OAE, whereas at Peniche, Portugal (Hermoso et al., 2009), and Monte Mangart, Julian Basin (Fig. 10) (Sabatino et al., 2009, 2011), organic-rich, basinal accumulations deposited during the OAE contain elevated Mn concentrations. The ferruginous, manganese-rich hardground of Monte Mangart is correlative to the ferruginous hardground of the Kovk section (Fig. 10), but the two display opposite responses in Mn concentrations as a result of differences in organic matter accumulation.

PALEOECOLOGICAL RESPONSE TO THE OAE

Monospecific brachiopod proliferation within early Toarcian discontinuity surfaces has also been documented on the SE part of the Adriatic Carbonate Platform (Črne, 2009; Črne & Goričan, 2008), and on the Lazio-Abruzzi Platform of the Italian Appenines (Graziano et al., 2006). This phenomenon has previously been attributed to platform drowning and meso-eutrophic conditions coincident with the early Toarcian OAE (Graziano et al., 2006). Our data generally agree with this interpretation, and provide a nuanced understanding of these disaster taxa. Sedimentologic and geochemical data indicate that the direct correspondence of these brachiopod beds with the early Toarcian OAE is likely a result of harsh environmental conditions that choked carbonate production on the platform. Heavily populated terebratulid beds likely reflect brief periods of oxygenation of the water column during an overall anoxic to euxinic regime throughout the OAE. The combination of relative deepening and meso-eutrophic conditions, along with higher calcite saturation relative to aragonite, provided the conditions necessary for these disaster taxa to proliferate. Accessory organisms include crinoids, which are likely transported from other intermittently oxygenated settings, as well as platycopid ostracods (Fig. 5E) that have previously been linked to dysaerobic conditions on the seafloor (Boomer & Whatley, 1992; Boomer et al., 2003; Horne et al., 2011).

A conspicuous turnover in the skeletal composition of the NW Adriatic Carbonate Platform occurs at the onset of the OAE: diverse aragonitic foraminiferal-mollusk-dasycladacean assemblages characterize the late Pliensbachian, whereas calcitic brachiopod-crinoid assemblages dominate the immediate OAE aftermath (Fig. 3). Mollusks and foraminifers return once again in the upper half of facies association 2a at Kovk, but they are generally auxiliary to the crinoid-brachiopod rich facies (Fig. 3). This

transition may be the result of changing paleoceonographic conditions and/or facies changes; however, a similar skeletal turnover in the early Toarcian assemblages of the SE margin of the Adriatic Carbonate Platform (Črne & Goriccan, 2008; Črne, 2009), and on the adjacent Trento platform ("Fanes Encrenite") (Masseti & Bottoni, 1978; Bosellini et al., 1981) (Figs. 10, 11) suggest that facies variability is likely subordinate to a fundamental shift in the dominant carbonate producing organisms in the region.

Though assessing the driver of this change is beyond the scope of this study, previous authors have speculated that the carbonate factory shutdown during the OAE was the result of ocean acidification followed by a carbonate overshoot in the form of an explosion of calcitic ooids on the adjacent Trento Platform (Trecalli et al., 2012). Assessing ocean acidification in deep time is incredibly difficult, because, in theory, an acidification event is non-preservational to destructive in nature (Kump et al., 2009; Greene et al., 2012; Honisch et al., 2012). We can, however, reasonably infer that due to the incredibly low carbonate accumulation rates following the shutdown of the carbonate factory on the Adriatic Carbonate Platform, there was a halt in carbonate production (regardless of whether or not water became undersaturated). Following this halt in carbonate precipitation, there was likely a large buildup of excess alkalinity, which would have caused an "overshoot" of saturation state and subsequently enhanced carbonate precipitation (Stanley & Hardie, 1998; Kump et al., 2009; Trecalli et al., 2012). The carbonate factory shutdown that drove this alkalinity buildup may have been caused by any combination of persistent deoxygenation of the water column and/or uppermost bottom sediment, partial drowning, eutrophication, and acidification, but the result was a proliferation of calcitic fauna and the explosion of calcitic ooids following the amelioration of paleoceanographic conditions. After this initial overshoot, the nature of

carbonate precipitation on the platform in terms of grain and skeletal composition was still markedly different than that prior to the OAE (Fig. 3).

The proliferation of ooids is represented by the Toarcian-Aalenian aged "Ternowaner Oolite" of the NW Adriatic Carbonate Platform (Kossmat, 1905; Bosellini et al., 1981; Winterer & Bosellini, 1981) and equivalent "San Vigilio Oolite" of the Trento Platform (Bosellini et al., 1981; Winterer & Bosellini, 1981; Trecalli et al., 2012). A similar phenomenon has been documented following several other major biotic crises that resulted in the prolonged suppression of skeletal carbonate production. In the wake of the end Permian extinction, for example, widespread calcitic and bimineralic oolites, including giant ooids, were deposited in the early Triassic (Payne et al., 2006; Pruss, et al., 2006; Lehrmann et al., 2012). Widespread oolite deposition also occurred in close stratigraphic proximity to the Wenlock-Ludlow extinction intervals of Sweden during a period otherwise characterized by a deficiency of ooids (Groves & Calner, 2004). On the Trento Platform, oolites prograded across a wide swathe of the platform in the immediate aftermath of the Mid Sinemurian carbon-cycle perturbation (Preto et al., 2017). As such, we interpret the "ooid dump" following the Toarcian OAE in the Adriatic region to reflect the continued suppression of skeletal carbonate production (Payne et al., 2006; Lehrmann et al., 2012). Skeletal carbonate accounts for a major carbonate sink, such that the reduction of this factor yielded higher alkalinity, promoting voluminous ooid precipitation for an extended period of time (Figs. 10, 11).

CONSEQUENCES OF THE LARGE IGNEOUS PROVINCE VOLCANISM

Percival et al. (2015, 2016) link globally enhanced mercury deposition at the Pliensbachian-Toarcian Event and the early Toarcian OAE to eruptions/emplacement of the Karoo-Ferrar LIP. This is the first study to recognize mercury enrichments in

association with the OAE in low TOC platformal carbonates. Furthermore, enrichments in mercury at Kovk occur in concert with the negative negative carbon isotope excursion demarcating the OAE (Fig. 8A). We, therefore, support the previously established conclusion that the paced eruption/emplacement of the Karoo-Ferrar-Chon Aike LIP was the trigger for the Toarcian OAE (e.g. Burgess et al., 2015). Enrichments after the OAE are likely related to continued volcanism in the Karoo-Ferrar-Chon Aike Large Igneous Province. The rapid introduction of isotopically light carbon (either by methane hydrate release, direct subaerial release of volcanic methane and carbon dioxide, or degassing of metamorphically altered carbon reservoirs) likely accounts for the negative carbon isotope excursion of the OAE (Hesselbo et al., 2000; Pálfy & Smith, 2000; McElwain et al., 2005; Beerling & Brentnall, 2007; Pieńkowski, et al., 2016; Svensen et al., 2007; Them et al., 2017). The ubiquity of this excursion in marine organic, marine carbonate, and terrestrial records gives testament to the truly global nature of this carbon cycle perturbation, the effects of which also had a global reach (Hermoso et al., 2008; Caruthers et al., 2013, 2014; Ikeda & Hori, 2014; Al-Suwaidi et al., 2016; Them et al., 2017).

Although the extent of the OAE and its characteristic negative carbon isotope excursion are global, the magnitude of the excursion itself is highly variable. In basinal sections at Yorkshire (Hesselbo et al., 2000; Kemp et al., 2005) and Monte Mangart (Fig. 10) (Sabatino et al., 2011), the magnitude of the negative excursion in organics reaches approximately 8‰, and 6‰, respectively. On the other hand, platformal sections from the Adriatic Carbonate Platform show negative isotope excursions in organics of 2.2‰ on the platform margin (this study), and approximately 3‰ within carbonates of the platform interior (Sabatino et al., 2013). Herein we discuss several possible sources for this variability.

The influence of carbonate on the organic carbon isotope profile of this study can be rejected as the source of the dampening of the negative isotope excursion because sample preparation was done so as to ensure the complete removal of carbonate, and the range of $d^{13}C$ values obtained closely match those of other organic values for the interval (e.g. Them et al., 2017). Furthermore, though significantly less than the excursions of some basinal section excursions, the dampened excursions on the outer and inner margins of the Adriatic Carbonate Platform suggest that the platformal excursion is inherently different for other reasons. A possible explanation is that the communities of organisms fixing carbon in the neritic versus pelagic realm were different. Variable $d^{13}C$ values for platformal versus basinal organic accumulations may be attributed to differences in the mass-dependent fractionation of carbon during photosynthesis between distinct communities. Studies of carbon isotope profiles derived from compound-specific biomarkers during the Toarcian OAE highlight variability in the negative carbon isotope excursion of different communities, lending credence to this interpretation (French et al., 2014; Schouten et al., 2000; Suan et al., 2015). The absolute magnitude of the carbon isotope excursion estimated from these studies was likely only 3-4‰ (Them et al., 2017), indicating that other factors are accountable for the disparity in carbon isotope records.

Regional variability in the amount and composition of dissolved inorganic carbon between platforms and shelves may have existed as a result of differences in planktonic communities as well as their abundance. Increased fixation of ^{12}C in the pelagic realm may have occurred around zones of upwelling, such as in the vicinity of Monte Mangart (Sabatino et al., 2009). As a result, the dissolved inorganic carbon pool from which neritic organisms were fixing carbon may have been preferentially enriched in ^{13}C, thus imparting a dampened negative isotope excursion on neritic organics. Upon deposition, basinal organic accumulations were likely deposited in anoxic to euxinic conditions

(Bellanca et al., 1999; Sabatino et al., 2009, 2011). Under these conditions, the presence of autotrophic bacteria such as nitrifying and sulfate reducing bacteria may be present (Fry et al., 1991). These organisms have very negative $d^{13}C$ values (Degens et al., 1968), and thus may have contributed to the amplification of the negative carbon isotope excursion in basinal sections relative to the excursions of the more intermittently oxygenated carbonate shelves.

The effect of volcanism on the carbon isotope mass-balance of the ocean-atmosphere system can be interpreted from the paired $d^{13}C$ curves for marine organics and carbonate. Kump & Arthur (1999) modeled the changes in the carbon isotopic composition of marine carbonate and organic matter in response to increases in the flux of volcanic carbon over an interval comparable to the length of the early Toarcian OAE (500 k.y.). A 50% increase in the volcanic carbon input almost doubles atmospheric pCO_2 and should intuitively drive depletion in the $d^{13}C$ of carbonate and organics as a result of the increased flux of isotopically light carbon into the system. However, the rise in pCO_2 also drives an increase in the difference between the $d^{13}C$ values of organics and carbonate, which actually opposes the depletion of the $d^{13}C$ values of carbonate (Kump & Arthur, 1999). The modeled response of the $d^{13}C$ ratios of marine organics and carbonate to the increased flux of volcanic carbon thus predicts a negative excursion in the organics, but a very dampened to non-existent excursion in carbonates (Kump & Arthur, 1999). This response can be seen in the $d^{13}C$ curves of organics and carbonate from the Adriatic Carbonate Platform during the OAE: the organics undergo a -2.2‰ excursion while the carbonates undergo virtually no excursion (Fig. 3). Though these data match the predicted response, the complete lack of a negative excursion in the carbonates disagrees with other $d^{13}C$ records of carbonates during the Toarcian OAE (e.g. Hesselbo et al., 2007; Bodin et al., 2016). We cannot account for this discrepancy, but speculate

that it may be a result of differing paleoceanographic conditions and diagenetic affects. Both the organic and carbonate curves, however, display the same globally recognized positive excursions following the maximum negative deflection in the organics. This response is related to globally enhanced carbon burial, which in turn caused a drawdown in atmospheric pCO_2 and depletion in the inventory of ^{12}C (Kump & Arthur, 1999).

Changes in the Composition of Marine Carbonate

In addition to the "ooid dump", a second peculiar phenomenon arose in the aftermath of the OAE: the majority of marine precipitates were calcitic. The distinct shift from aragonitic to calcitic skeletal fauna between the Pliensbachian and early Toarcian (Fig. 3) is characterized by the predominance of calcitic organisms such as brachiopods, crinoids, calcispheres, nodosariid foraminifera, and ostracods, with few aragonitic organisms preserved including juvenile ammonites and thin-shelled bivalves. Furthermore, ooids and cements in the strata overlying the OAE are overwhelmingly calcitic. The first noticeable pseudomorphs after aragonite are acicular isopachous cements that appear at 38.4 m (Fig. 6F), well after the OAE. Given these lines of evidence, we interpret calcite to be the favored marine precipitate in the aftermath of the OAE. Though not surprising that calcite precipitates are abundant, given the transitional state of the Lower Jurassic between calcite and aragonite seas (Sandberg, 1983; Stanley & Hardie, 1998) the paucity of aragonite is peculiar. This peculiarity is not exclusive to the Toarcian of the Adriatic Carbonate Platform. On the Cretaceous Comanche Shelf of Texas and the Gulf of Mexico, in the aftermath of OAE 1a and OAE 1b, calcitic fauna such as oysters and the foraminifera *Orbitolina* proliferate (Phelps et al., 2015) and there is a paucity of aragonite cement pseudomorphs (pers comm. Charlie Kerans, 2016).

Rigorously assessing the cause of this apparent shift in mineralogy is beyond the scope of this study, however, several possible drivers can be considered. Aragonite versus calcite precipitation is broadly governed by the saturation state of seawater with respect to calcite and aragonite (Kump et al., 2009; Honisch et al., 2012), the amount of Mg in solution, temperature, pH, and the presence of ions Sr, Ba, Pb, and Na (Milliman, 1974). Calcite is favored when there is no Mg in solution, when temperatures are relatively low, pH is lower, and Na is available (Milliman, 1974). The saturation state of seawater (Ω) with respect to calcite and aragonite is dependent upon the concentration of ions Ca^{2+} and CO_3^{2-} and the individual solubility product constants of aragonite and calcite (K_{SP}) (Ridgwell & Zeebe, 2005). Because the K_{SP} of calcite and aragonite are only slightly different, their saturation state in seawater differs by only 1-2 Ω (Mucci, 1983). Given that ooid precipitation occurs at a minimum saturation state of $\Omega_{aragonite.} = 4$ (Opdyke & Wilkinson, 1990), there is no possible way that with the plethora of calcitic ooids being formed following the Toarcian OAE, seawater was undersaturated with respect to aragonite, but supersaturated with respect to calcite.

Another possible driver for the predominance of calcite following these events could be temperature, however, the subtropical paleolatitudinal position of the Adriatic Carbonate Platform in the Lower Jurassic (Suan et al., 2008), and the Comanche Shelf during the Aptian-Albian (Phelps et al., 2014) likely provided the temperatures conducive to both calcite and aragonite precipitation. The pH of seawater is also unlikely to blame because it is related to the availability of CO_3^{2-} in the oceans (Ridgwell & Zeebe, 2005), which in part controls the carbonate saturation of seawater with respect to aragonite and calcite, as explained above. Furthermore, buffering of pH so as to influence the precipitation of calcite over aragonite over the tens, to hundreds of thousands of year intervals that we are considering is highly unlikely. Lastly, Sr, Ba, Pb, and Na have a

much lower order control on carbonate precipitation than the more major ion, Mg (Milliman, 1974). We thus interpret the relative availability of Mg in the oceans to be a possible driver of the calcite phenomenon.

The Mg^{2+}/Ca^{2+} ratio of seawater affects the kinetics of calcite precipitation such that a higher ratio is inhibiting (Milliman, 1974). Furthermore, this ratio has changed throughout time and is widely believed to be a major driver in the secular oscillations of carbonate mineralogy throughout the Phanerozoic (calcite versus aragonite seas) (Stanley & Hardie, 1998; Stanley et al., 2010; Lehrmann et al., 2012). Changes in the Mg^{2+}/Ca^{2+} ratio of seawater are largely related to the rate of global seafloor spreading (Stanley & Hardie, 1998); Demicco et al., 2005; Stanley et al., 2010) because the hydrothermal interaction of basalt with seawater leads to the formation of Mg-silicate minerals through the process of serpentinization. Thus during times of high rates of seafloor spreading, the [Mg] of seawater is lowered, yielding predominantly "calcite" seas in an overall "greenhouse" climate.

Though these secular oscillations occur over long extended periods throughout the Phanerozoic (Sandberg, 1983; Stanley & Hardie, 1998), we hypothesize that the Mg^{2+}/Ca^{2+} of seawater may have been ephemerally altered to an extremely low value during periods of enhanced submarine volcanism in the Mesozoic. Instances of anomalously low Mg^{2+}/Ca^{2+} may have coincided with instances of enhanced large igneous province volcanism, because large igneous province emplacement itself is associated with expedited seafloor spreading. Furthermore, large igneous province activity is widely accepted as the causal mechanism for Mesozoic OAEs (Sinton & Duncan, 1997; Larson & Erba, 1999; Pálfy & Smith, 2000; Weissert & Erba, 2004; Kuroda et al., 2007; Svensen et al., 2007; Burgess et al., 2015). We thus propose that large igneous province volcanism associated with OAEs may have lowered the Mg^{2+}/Ca^{2+} of seawater for short

intervals, such that calcite was the heavily favored marine precipitate in the aftermath of OAEs.

Platform Architecture

The Pliensbachian sedimentary record of the NW margin of the Adriatic Carbonate Platform reflects a healthy carbonate factory with an abundant and diverse skeletal assemblage (Fig. 3). Notably, massive aragonitic calcification is recorded in coral patch reefs (Turnšek, 2003), dasycladacean meadows, and lithiotid biostromes (Debeljak, and Buser, 1997). Carbonate factory demise at the onset of the OAE was likely caused by deoxygenation of the water column, and may have been supplemented by acidification and eutrophication. It is expressed sedimentologically by the ferruginous hardground interval, which represents a major discontinuity (Figs. 3, 10). With no carbonate production to keep up with the concomitant eustatic sea-level rise and normal subsidence on the platform, the Trnovski Gozd area shifted from a shallow subtidal setting to an environment below fair weather wave base (Fig. 10). Stacked, crinoidal-ooid grainstones reflect transport from encrinitic-ooid shoals that developed on the outer shelf, similar to the Fanes Encrinite and San Vigilio Oolite of the Trento Platform (Fig. 11) (Masseti & Bottoni, 1978; Bosellini et al., 1981), and may have been influenced by the increased hurricane intensity and frequency in the early Toarcian (Krencker et al., 2015).

At the same time, the platform interior shifted to a deeper, deoxygenated, low diversity environment expressed by the early Toarcian spotted limestones (Figs. 7, 10). This sickly facies spans the entire Toarcian interval, up to 100 m at Velebit, Croatia (Tišljar et al., 2002), indicating that the onset of the OAE, coupled with differential subsidence, not only instigated the restricted circulation of the platform interior, but significantly influenced the conditions necessary for the existence of an intrashelf basin

long after the OAE. Following the immediate aftermath of the OAE, shelf edge crinoidal-oolitic grainstone development on the Adriatic Carbonate Platform continued (Figs. 3, 10). By the end of the Toarcian, the Trento Platform subsided to a submarine plateau, making the NW margin of the Adriatic Carbonate Platform a windward margin and hyperactive ooid factory (Figs. 10, 11) (Bosellini et al., 1981; Winterer & Bosellini, 1981). An oolitic basin floor fan prograded west across the Belluno Basin, and was sourced from the NW Adriatic Carbonate Platform Ternowaner Oolite (Figs. 10, 11) (Bosellini et al., 1981). On the platform, the eastward progradation of the Ternowaner Oolite led to cessation of spotted limestone deposition by the Middle Jurassic (Tišljar et al., 2002), finally allowing a flat-topped carbonate platform to reestablish.

An Ecoeustatic Regime Variable

Intrashelf basin development as a result of a depressed carbonate factory has also been documented at OAE1d in the Arabian Carbonate Platform (Van Buchem, et al., 2002; De Keyser & Kendall, 2014; Vahrenkamp et al., 2015) and can be attributed to greater circulation on the platform margins, coupled with a normally subsiding platform interior. A similar mechanism likely led to the development of the Cretaceous Maverick intrashelf basin of the Northern Gulf of Mexico (Phelps et al., 2014; Sitgreaves, 2015), and suggests that OAEs play an important role in shaping the architectural development of carbonate platforms. Major discontinuities have preceded intrashelf basin development (De Keyser & Kendall, 2014), and have long been recognized as drowning unconformities on carbonate platforms (e.g. Goldhammer et al., 1990; Schlager, 1989; Graziano, 1999; Léonide et al., 2012). By tying carbon isotope stratigraphy to discontinuities, we are able to recognize the coincidence of biotic crises such as OAEs

with major drowning unconformities (e.g. Weissert et al., 1998; Léonide et al., 2012; Godet, 2013; Phelps et al., 2014, 2015).

A nuanced understanding of the shutdown of carbonate factories resulting in drowning unconformities at OAEs is furthered by the results of this study: the combination of an extended period of deoxygenation, alkalinity crisis, and eutrophication throttled carbonate production, leading to sediment starvation and the development of a drowning unconformity. Remarkably similar stratigraphic surfaces are recognized for this interval throughout the carbonate platform of the Southern Provence sub-Basin (Léonide et al., 2012), and at Monte Kumeta, Italy (Mallarino et al., 2002), and on the adjacent Julian High (Fig. 10) (Šmuc & Goričan, 2005; Sabatino et al., 2011). The development of these surfaces has been related to eutrophication and deoxygenation coincident with the Pliensbachian-Toarcian Event and the early Toarcian OAE. The same echinoid-rich deposition occurred at both of these localities, and has been ascribed a depositional water depth of less than 23 m (Mallarino et al., 2002). On the Adriatic Carbonate Platform, the basinward extent of the drowning unconformity transitions into a condensed section that includes OAE organic carbon-rich black shales (Jenkyns et al., 1985; Bellanca et al., 1999). Towards the inner part of the platform the drowning unconformity transitions to an organic-rich intrashelf basin fill. The drowning unconformity itself developed as a result of the cessation of carbonate production, followed by normal rates of subsidence and eustatic sea-level rise. Depositional water-depth quantification at Monte Kumeta indicate that sea level rise did not exceed 7 m/m.y. (Mallarino et al., 2002), suggesting that a force other than just drowning caused the carbonate platform demise at the OAE. Had the OAE not crippled the factory, carbonate production would have kept up with relative sea-level rise. Evidently this “ecoeustatic” signal (Sitgreaves, 2015) had a profound impact on the architectural development of not only the Adriatic Carbonate

Platform, but western Tethyan platforms in general. The wide distribution of the drowning unconformity in the western Tethys supports the sequence stratigraphic relevance of these surfaces. Recognizing drowning unconformities as a product of this ecoeustatic signal may enable the prediction of time equivalent up and downdip stratigraphy. The potential utility of this approach and the now widely recognized influence of OAEs and other biotic crises on platform architecture warrants the consideration of the ecoeustatic effect as a serious regime variable in carbonate sequence stratigraphy. Biotic crises have been affecting carbonate production for the entirety of the Phanerozoic. Therefore, the ecoeustatic regime variable has been a major control of carbonate sequence stratigraphy throughout the Phanerozoic.

CONCLUSIONS

The Adriatic Carbonate Platform presents a record of major paleoceanographic changes coincident with the early Toarcian OAE. These changes were triggered by activity in the Karoo-Ferrar-Chon Aike large igneous province, as evidenced by globally distributed mercury enrichments within the OAE interval. Anoxic to euxinic conditions persisted both in the adjacent basin and on the platform, and were likely exacerbated by eutrophication. The NW margin of the Adriatic Carbonate Platform, which was a healthy and diverse metazoan flat-topped carbonate platform in the Pliensbachian, partially drowned in the early Toarcian as a result of the carbonate factory collapse and concomitant sea-level rise during the OAE. The inner platform accumulated a thicker section during the OAE as a result of differential subsidence. Redox sensitive element enrichments, particularly sustained Fe enrichment, indicate a prolonged period of deoxygenation of the shelf. Depletions in redox sensitive trace metals following the onset of the OAE reflect a global drawdown in the trace element inventory of seawater due to the sequestering of these metals during the global deposition of black shales. Intrashelf basin-fill on the Adriatic carbonate platform occurred under a euxinic regime throughout the Toarcian stage, while the platform margin slowly recovered with the production of predominantly calcitic fauna and ooids. The filling of the intrashelf basin and recovery of normal carbonate accumulation by the end of the Toarcian led to the reestablishment of a normal flat-topped carbonate platform.

The detailed assessment of the Adriatic Carbonate Platform evolution across the Toarcian Oceanic Anoxic Event presented here adds to a growing body of literature supporting the intrinsic control that OAEs and other biotic crises exert on platform architecture. OAEs are not solely deep-water phenomena, and can have distinctive

expressions in shallow-water settings. Understanding the linkage between deep-water and shallow-water sedimentation across OAEs, as well as the associated geochemical changes, is an essential step towards understanding the sequences stratigraphic control that OAEs have on carbonate and mixed carbonate/siliciclastic systems.

APPENDIX

TABLES

Sample Height (m)	$\delta^{13}C_{org}$ (VPDB)	% Carbon	$\delta^{13}C_{carb}$ (VPDB)	$\delta^{18}O_{carb}$ (VPDB)
0.00	-26.20	0.004	-	-1.23
1.77	-26.81	0.005	2.37	-0.62
3.30	-26.60	0.006	2.33	-0.33
4.00	-27.17	0.015	1.59	-0.72
5.90	-27.84	0.009	1.77	-1.33
6.09	-27.00	0.009	1.64	-0.85
6.35	-26.88	0.009	1.47	-1.34
6.37	-27.99	0.010	1.96	-0.83
7.13	-26.97	0.009	1.42	-0.97
7.24	-27.57	0.009	1.72	-1.16
8.06	-27.53	0.012	1.22	-1.58
8.49	-26.93	0.006	2.03	-0.59
9.08	-27.88	0.010	1.97	-0.70
10.18	-27.28	0.007	1.60	-1.65
10.38	-27.98	0.003	2.10	-0.93
10.45	-26.89	0.002	2.18	-1.99
10.79	-	0.009	-	-
10.98	-27.82	0.010	2.52	-0.77
11.38	-27.72	0.009	2.45	-0.50
11.88	-26.99	0.008	2.46	-0.49
11.99	-26.65	0.012	-	-
12.20	-28.52	0.009	-	-
12.61	-28.57	0.014	2.43	-0.97
13.18	-28.88	0.012	2.34	-1.55
13.45	-28.42	0.010	2.67	-1.05
13.95	-28.19	0.011	2.92	-0.91
14.25	-27.10	-	3.10	-1.08
14.54	-26.11	0.004	3.34	-0.82
15.03	-25.60	0.017	3.52	-1.26
15.38	-27.12	0.010	3.55	-0.85
15.51	-27.71	0.010	3.56	-1.07
16.35	-27.71	0.010	2.12	-1.83
16.99	-26.86	0.005	-	-
18.02	-27.07	0.012	-	-
19.51	-27.57	0.009	2.59	-1.43
21.54	-27.27	0.012	-	-
23.53	-27.83	0.013	2.97	-1.20
25.65	-26.63	0.012	3.12	-1.02
27.09	-26.72	0.018	3.08	-0.59
27.85	-27.42	0.017	2.95	-0.69
29.63	-27.65	0.016	2.99	-0.31
30.06	-27.47	0.018	3.10	-0.62
30.49	-27.79	0.016	3.06	-0.29
30.66	-27.28	0.022	3.11	-0.44
31.36	-27.14	0.014	3.13	-0.46
31.77	-28.13	0.007	2.68	-0.84
32.38	-28.02	0.009	1.47	-1.17
33.11	-28.09	0.016	2.83	-0.50
33.53	-28.16	0.010	-	-
33.91	-27.63	0.010	2.83	-0.82

Table 1: Compilation of stable carbon and oxygen isotope data and total organic carbon for the Kovk section (continued on next page).

Sample Height (m)	$\delta^{13}C_{org}$ (VPDB)	% Carbon	$\delta^{13}C_{carb}$ (VPDB)	$\delta^{18}O_{carb}$ (VPDB)
35.49	-27.48	0.010	2.64	-0.55
38.09	-27.83	0.005	2.49	-1.00
38.99	-27.74	0.008	2.58	-0.44
39.47	-27.93	0.007	2.36	-0.38
40.28	-26.79	0.008	2.40	-0.40
40.69	-26.86	0.009	2.67	-0.42
41.15	-27.28	0.007	2.25	-1.19
41.81	-26.65	0.007	2.34	-0.71
42.64	-26.47	0.002	2.43	-0.27
44.83	-26.69	0.004	2.15	-1.41
46.37	-27.94	0.005	2.46	-0.78
47.22	-25.69	0.005	2.68	-0.22
47.96	-26.88	0.006	2.50	-0.55

Table 1 continued

Sample Height (m)	Major							Trace				
	Ca (%)	Mg (%)	Al (%)	Ti (%)	P (%)	Fe (%)	Mn (ppm)	Ba (ppm)	V (ppm)	Ni (ppm)	Mo (ppm)	Hg (ppb)
0.00	38.43	0.23	0.11	0.00	0.01	0.26	187	125	-	7	-	0.00
1.77	37.53	0.17	0.05	0.00	0.02	0.24	189	100	-	9	1	0.37
3.30	38.10	0.20	0.02	0.00	0.02	0.24	189	92	-	9	-	0.48
4.00	-	-	-	-	-	-	-	-	80	-	-	0.53
4.00	37.10	0.21	0.26	0.01	0.02	0.31	186	126	-	8	1	0.00
5.59	-	-	-	-	-	-	-	-	81	-	-	0.31
5.90	38.32	0.22	0.06	0.00	0.01	0.24	189	111	-	11	1	0.71
6.08	-	-	-	-	-	-	-	-	79	-	-	1.18
6.09	38.86	0.19	0.06	0.01	0.01	0.24	188	79	-	7	4	0.43
6.35	38.32	0.21	0.04	-	0.01	0.24	189	125	-	11	1	0.31
6.37	37.04	0.19	0.18	0.01	0.02	0.26	188	108	-	15	0	1.09
7.03	-	-	-	-	-	-	-	-	81	-	-	0.25
7.13	-	-	-	-	-	-	-	-	80	-	-	-
7.13	37.43	0.16	0.02	-	0.02	0.23	189	75	-	8	3	0.45
7.24	38.80	0.21	0.06	0.00	0.01	0.24	188	102	-	10	1	0.27
8.06	38.19	0.21	0.04	0.00	0.01	0.24	188	93	-	12	4	1.48
8.08	-	-	-	-	-	-	-	-	79	-	-	0.35
8.49	38.68	0.22	0.06	0.00	0.01	0.24	189	103	-	9	2	0.39
8.53	-	-	-	-	-	-	-	-	87	-	-	0.24
8.88	-	-	-	-	-	-	-	-	78	-	-	0.24
9.08	37.94	0.20	0.08	0.00	0.02	0.26	188	115	-	10	4	0.28
9.58	-	-	-	-	-	-	-	-	88	-	-	0.43
9.84	-	-	-	-	-	-	-	-	79	-	-	0.57
10.18	37.65	0.13	0.04	0.00	0.02	0.23	189	147	-	9	1	0.53
10.38	38.47	0.16	0.04	0.00	0.01	0.23	189	105	-	10	0	0.46
10.45	38.11	0.16	0.02	0.00	0.02	0.24	190	87	-	9	1	0.52
10.98	38.20	0.19	0.04	-	0.02	0.24	189	121	-	12	1	0.91
11.38	-	-	-	-	-	-	-	-	80	-	-	0.56
11.38	38.00	0.18	0.04	-	0.01	0.24	189	118	-	9	8	0.41
11.88	37.92	0.17	0.05	0.00	0.02	0.24	189	100	-	10	4	1.56
11.99	38.70	0.18	0.06	0.00	0.01	0.26	188	104	-	10	7	1.34
12.20	33.60	0.34	0.83	0.05	0.03	0.39	178	159	-	11	3	4.63
12.40	-	-	-	-	-	-	-	-	63	-	-	3.55
12.61	37.97	0.19	0.10	0.00	0.01	0.23	187	125	-	11	0	0.34
13.18	36.66	0.20	0.27	0.02	0.04	0.49	184	112	-	10	-	1.42
13.45	35.81	0.17	0.18	0.01	0.03	0.56	189	98	-	12	-	1.27
13.45	-	-	-	-	-	-	-	-	65	-	-	0.53
13.95	39.08	0.27	0.22	0.02	0.02	0.32	185	87	-	13	5	2.49
14.25	38.79	0.24	0.14	0.00	0.01	0.26	186	158	-	12	1	0.99
14.34	-	-	-	-	-	-	-	-	72	-	-	2.28
14.54	36.04	0.23	0.54	0.03	0.02	0.46	180	139	-	11	1	2.89
15.03	40.79	0.31	0.10	0.02	0.01	0.29	183	47	-	11	4	0.58
15.13	-	-	-	-	-	-	-	-	79	-	-	2.56
15.38	37.78	0.15	0.14	0.01	0.02	0.29	186	116	-	11	1	3.55
15.51	40.59	0.32	0.12	0.01	0.00	0.28	186	140	-	9	-	0.87
15.59	-	-	-	-	-	-	-	-	78	-	-	4.55
16.35	37.58	0.44	0.10	0.00	0.02	0.32	186	145	-	10	5	3.70
16.54	-	-	-	-	-	-	-	-	82	-	-	1.98
16.99	39.91	0.54	0.11	0.01	0.01	0.27	187	82	-	10	5	1.38
18.02	37.19	0.62	0.04	0.00	0.02	0.24	188	97	-	9	3	3.01

Table 2: Compilation of elemental data for the Kovk section (continued on next page).

Sample Height (m)	Major							Trace				
	Ca (%)	Mg (%)	Al (%)	Ti (%)	P (%)	Fe (%)	Mn (ppm)	Ba (ppm)	V (ppm)	Ni (ppm)	Mo (ppm)	Hg (ppb)
18.07	-	-	-	-	-	-	-	-	81	-	-	1.57
18.28	-	-	-	-	-	-	-	-	83	-	-	1.20
19.51	37.41	0.87	0.07	0.00	0.02	0.27	186	125	-	8	0	2.43
19.89	-	-	-	-	-	-	-	-	92	-	-	1.21
20.15	-	-	-	-	-	-	-	-	79	-	-	1.28
21.41	-	-	-	-	-	-	-	-	95	-	-	0.94
21.54	32.76	2.89	0.06	0.01	0.02	0.29	184	125	-	5	0	1.32
21.64	-	-	-	-	-	-	-	-	92	-	-	0.67
23.43	-	-	-	-	-	-	-	-	83	-	-	0.47
23.53	35.70	0.71	0.01	0.00	0.02	0.26	188	101	-	10	0	0.70
23.91	-	-	-	-	-	-	-	-	83	-	-	2.54
25.65	37.57	0.19	0.10	0.00	0.02	0.28	187	132	-	10	3	0.31
25.68	-	-	-	-	-	-	-	-	81	-	-	0.47
27.07	-	-	-	-	-	-	-	-	75	-	-	0.62
27.09	39.71	0.26	0.10	0.01	0.01	0.26	186	121	-	11	-	1.02
27.85	38.46	0.18	0.16	0.01	0.02	0.37	184	121	-	13	3	0.72
29.63	36.16	0.24	0.53	0.02	0.03	0.39	181	192	-	10	-	0.45
30.06	37.48	0.17	0.11	0.00	0.02	0.27	188	121	-	9	-	0.61
30.14	-	-	-	-	-	-	-	-	77	-	-	0.76
30.49	34.87	0.01	-	0.00	0.02	0.30	188	85	-	11	2	0.54
30.66	37.13	0.22	0.16	0.01	0.02	0.28	186	124	-	10	5	0.73
30.71	-	-	-	-	-	-	-	-	79	-	-	0.33
31.36	37.49	0.20	0.12	0.01	0.02	0.25	188	99	-	10	-	0.39
31.77	38.00	0.24	0.11	0.00	0.02	0.25	187	111	-	12	4	0.26
32.16	-	-	-	-	-	-	-	-	81	-	-	0.55
32.38	39.25	0.21	0.07	0.00	0.01	0.24	188	121	-	12	1	1.10
33.11	39.36	0.21	0.06	0.00	0.01	0.24	188	123	-	9	2	0.98
33.53	37.74	0.42	0.04	0.00	0.02	0.30	186	96	-	11	3	1.04
33.77	-	-	-	-	-	-	-	-	82	-	-	0.74
33.91	39.44	0.22	0.08	0.01	0.02	0.25	188	103	-	9	1	0.58
35.49	38.72	0.24	0.09	0.01	0.02	0.26	186	109	-	9	0	2.03
35.55	-	-	-	-	-	-	-	-	80	-	-	1.78
38.09	37.55	0.17	0.02	0.00	0.02	0.24	190	93	-	8	1	0.73
38.40	-	-	-	-	-	-	-	-	80	-	-	0.85
38.99	38.71	0.18	0.05	0.00	0.02	0.24	188	137	-	9	3	1.32
39.47	39.01	0.22	0.07	0.00	0.01	0.25	188	109	-	8	2	0.86
39.48	-	-	-	-	-	-	-	-	79	-	-	0.93
40.28	38.15	0.20	0.06	0.00	0.02	0.24	188	109	-	9	-	0.65
40.69	38.17	0.16	0.03	0.01	0.02	0.24	189	74	-	10	-	0.82
40.86	-	-	-	-	-	-	-	-	83	-	-	1.64
41.15	38.59	0.19	0.05	0.00	0.02	0.28	187	108	-	12	-	4.29
41.61	-	-	-	-	-	-	-	-	81	-	-	2.17
41.81	38.02	0.19	0.03	0.00	0.02	0.23	188	90	-	9	5	2.46
42.64	38.69	0.20	0.07	0.00	0.02	0.25	187	118	-	8	-	0.74
44.83	38.27	0.15	0.04	0.00	0.02	0.23	189	83	-	10	1	0.91
46.37	37.69	0.17	0.04	0.00	0.03	0.25	188	92	-	12	0	4.55
47.19	-	-	-	-	-	-	-	-	80	-	-	1.57
47.22	38.21	0.17	0.05	0.00	0.01	0.23	188	107	-	11	2	1.74
47.96	37.76	0.14	0.03	0.00	0.04	0.24	187	105	-	12	2	10.25
48.11	-	-	-	-	-	-	-	-	81	-	-	8.31

Table 2 continued

FIGURES

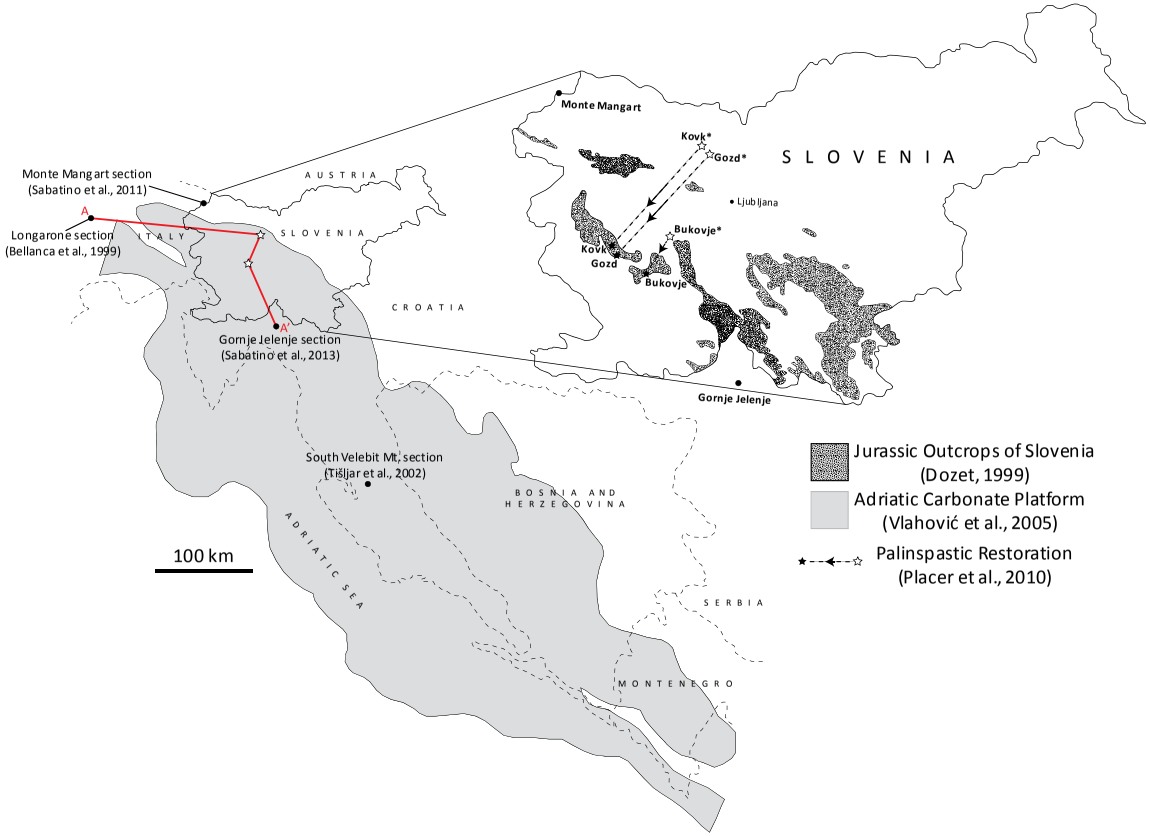

Figure 1: Current location of the Adriatic Carbonate Platform, modified from Vlahović et al. (2005). Inset of Slovenia outlines Lower Jurassic outcrops from Dozet (1997) and the Slovenian study localities. Palinspastic restorations of the Kovk, Gozd, and Bukovje localities are from Placer et al. (2010). Locations of important previoulsy published Lower Jurassic sections referenced in this study are labeled. Line A-A' indicates the location of sections in Figure 9.

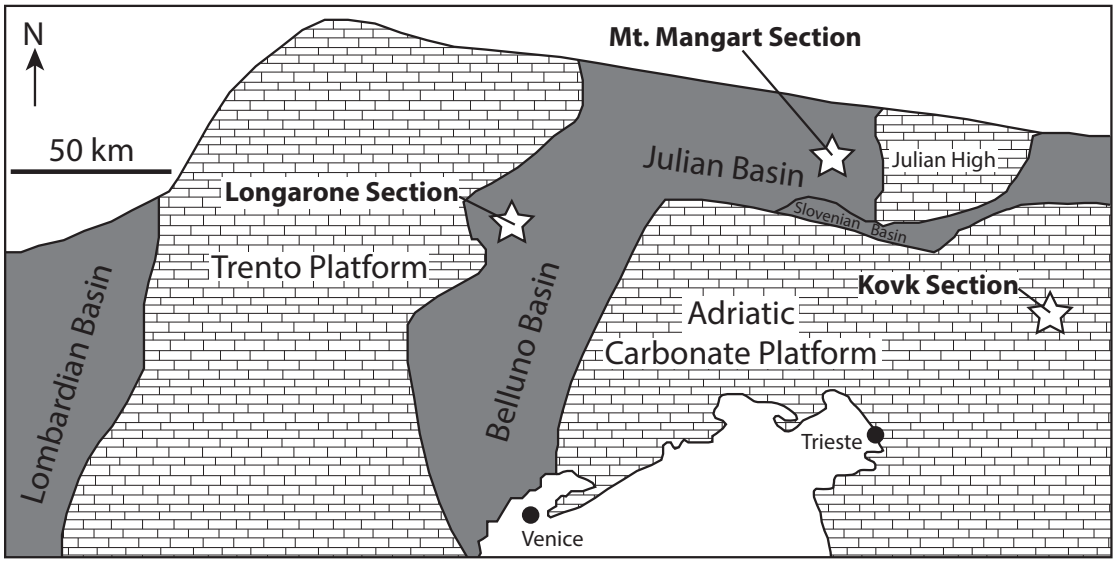

Figure 2: Paleotectonic configuration of the Southern and Dinaric Alps during the Lower Jurassic, showing the locations of platforms, basins, and studied sections. Figure modified from Sabatino et al. (2011); stars indicate the locations of sections in Fig. 10.

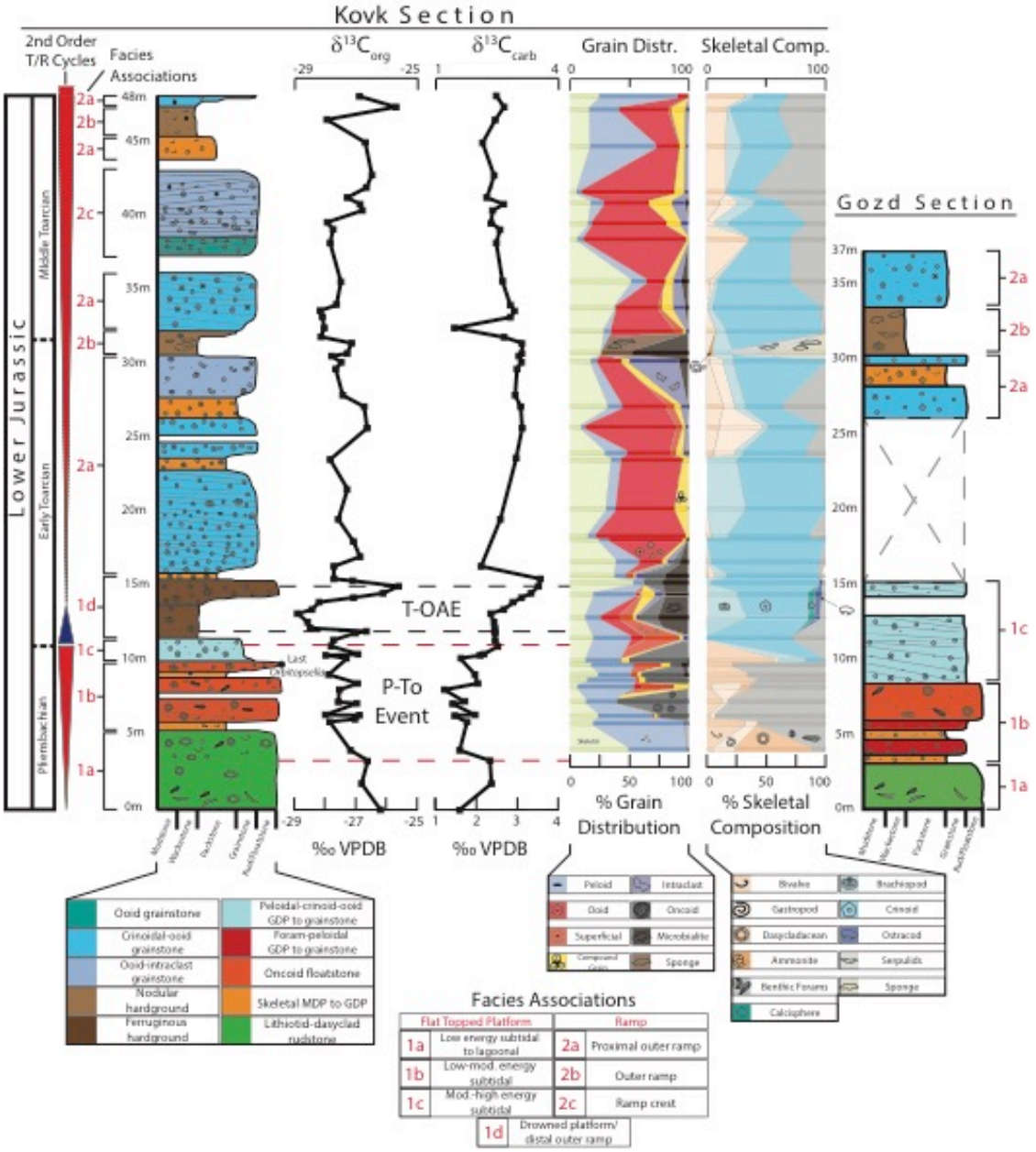

Figure 3: Lithostratigraphy of Trnovski Gozd, Slovenia, including the Kovk and Gozd measured sections. Facies associations and interpreted 2nd order transgressive/regressive (T/R) cycles of Hardenbol et al. (1998) are provided adjacent to each section. d13Corg and d13Ccarb isotope curves for the Kovk section are shown along with the stratigraphic location of the Pliensbachian-Toarcian event, and the early Toarcian OAE. Grain distribution and skeletal composition determined from the petrography the Kovk section are organized stratigraphically.

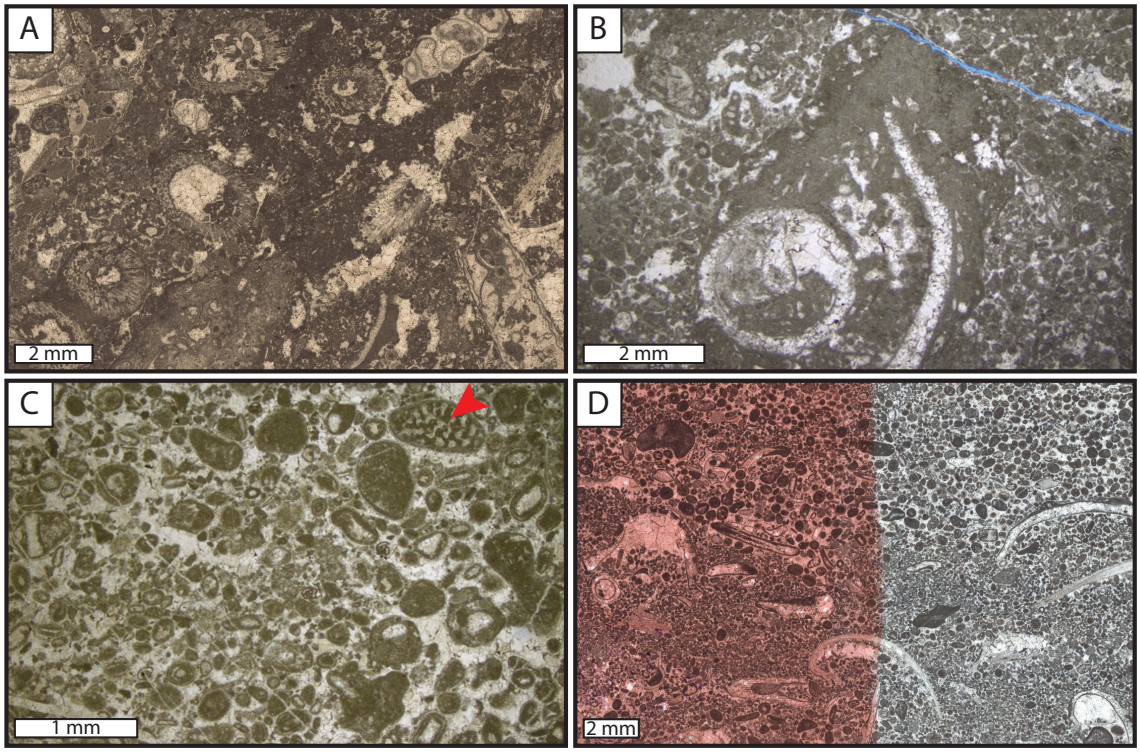

Figure 4: Pliensbachian microfacies of Kovk, Trnovski Gozd; all photomicrographs taken in plane polarized light. A) 4.00 m, facies association 1a: Gastropod – Palaeodasycladus mediterraneus float- to rudstone. B) 7.03 m, facies association 1b: Oncoid floatstone with a mollusc - foraminiferal - peloidal mud-dominated packstone matrix. C) 8.88 m, facies association 1b: mollusc - peloidal - foraminiferal grain-dominated packstone. White arrow points to a fragment of Orbitopsella. D) 9.84 m, facies association 1b: stratified gastropod - bivalve - superficial ooid - peloidal grainstone.

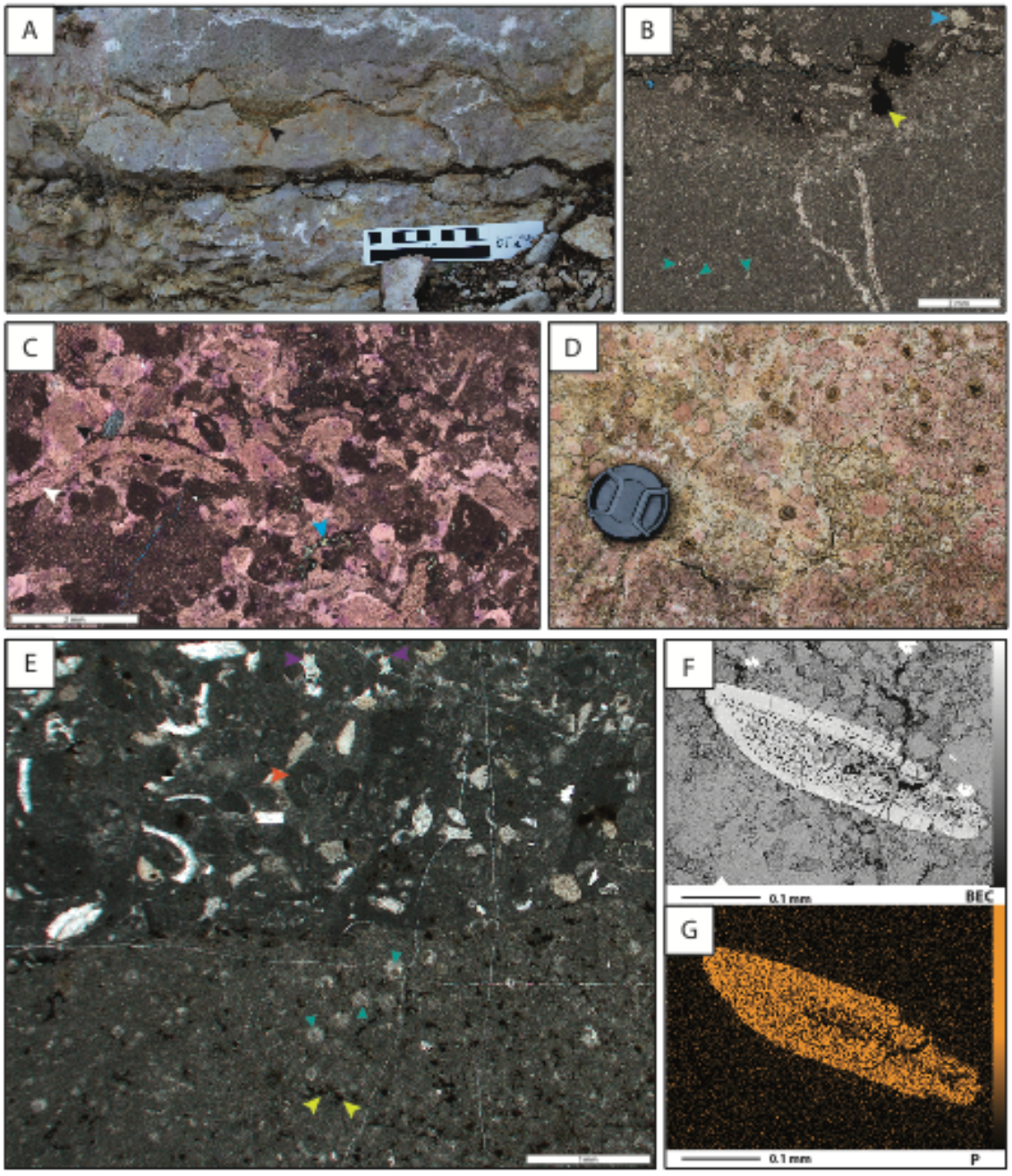

Figure 5

Figure 5 (previous page): Outcrop, microfacies, and EDS maps of the ferruginous hardground OAE interval at Kovk; all photomicrographs taken in plane polarized light. A) Hardground in outcropt at approximately 12.5 m. Stylotization is common, and concentrates insoluble glauconite (black arrow). Small ruler gradations = 1 cm. B) 13.45 m: wackstone to mud-dominated packstone. Blue arrow points to a crinoid fragment, yellow arrow to sub-millimetre, round, oxidized pyrite, and the teal arrow to calcispheres. The dashed line outlines a dissolution front that truncates a replaced grain. C) 14.34 m: microbial - brachiopod – crinoid mud-dominated packstone. The purple pigment indicates ferroan calcite that has reacted with potassium ferricyanide. White arrow points to a ferroan brachiopod, the black arrow to a ferroan crinoid and its ferroan syntaxial cement, and the blue arrow points to glauconite. D) Outcrop of ferruginous terebratulid brachiopod bed at 14.0 m. Lens cap is approximately 5 cm in diameter E) Hardground sample showing an erosive contact between a framboidal pyrite-rich, calcisphere wackestone (quiet sedimentation) and overlying ammonite – ostracod – crinoid mud dominated packstone (event sedimentation). Yellow arrows point to pyrite framboids, teal arrows to calcispheres, red arrow to juvenile ammonite, and purple arrows to platycopid ostracods. F) Backscatter compositional mode (BEC) image of bone with marrow preserved in center. G) EDS map of bone (Fig. 5F) indicating high phosphorous content.

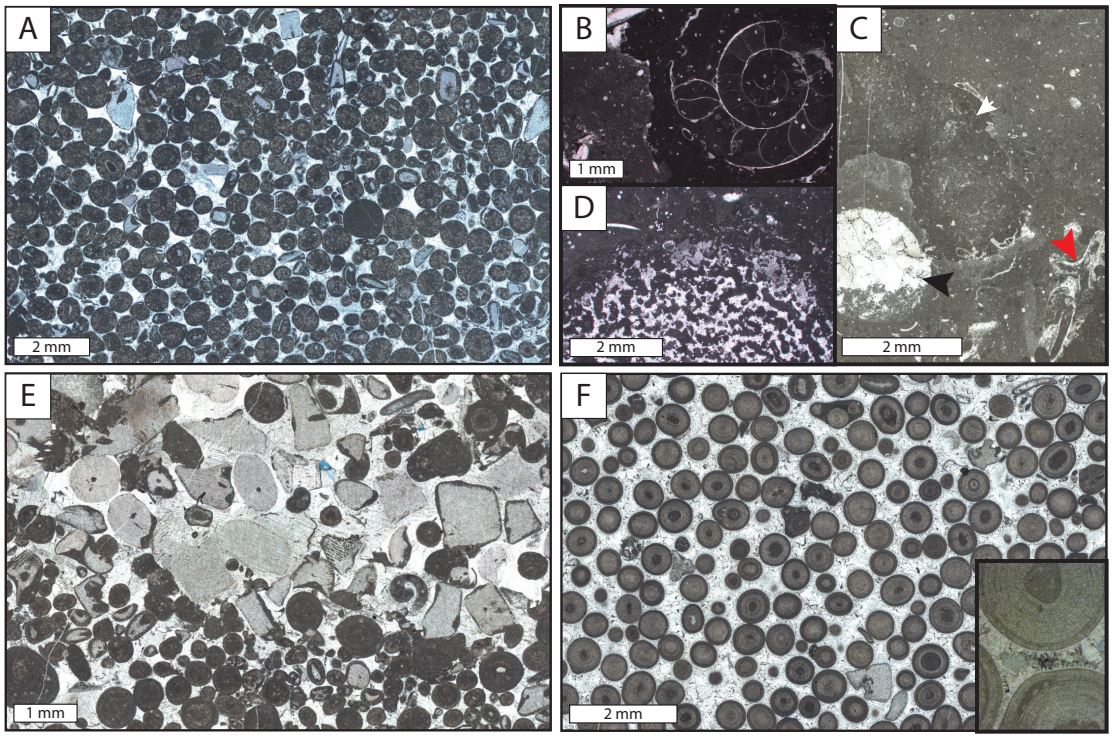

Figure 6: Post-OAE Toarcian microfacies; all photomicrographs taken in plane polarized light.A) 25.68 m in section, facies association 2a: crinoidal – radial ooid grainstone. Note minor fitting and compaction of grains owing to a lack of isopachous cement. B-D) 30.71 m in section, facies association 2b: B) Juvenile ammonite. C) White arrow points to sponge, red arrow to serpulid worm tubes, and black to an uncompacted burrow with geopetal fecal pellet fill. D) Calcisponge in a spiculitic mud matrix. E) 33.77 m in section, facies association 2a: stratified ooid-crinoid grainstone. F) 38.40 m in section, facies association 2c: moderately sorted ooid grainstone. Note lack of compaction owing to acicular isopachous fibrous marine cements (see inset).

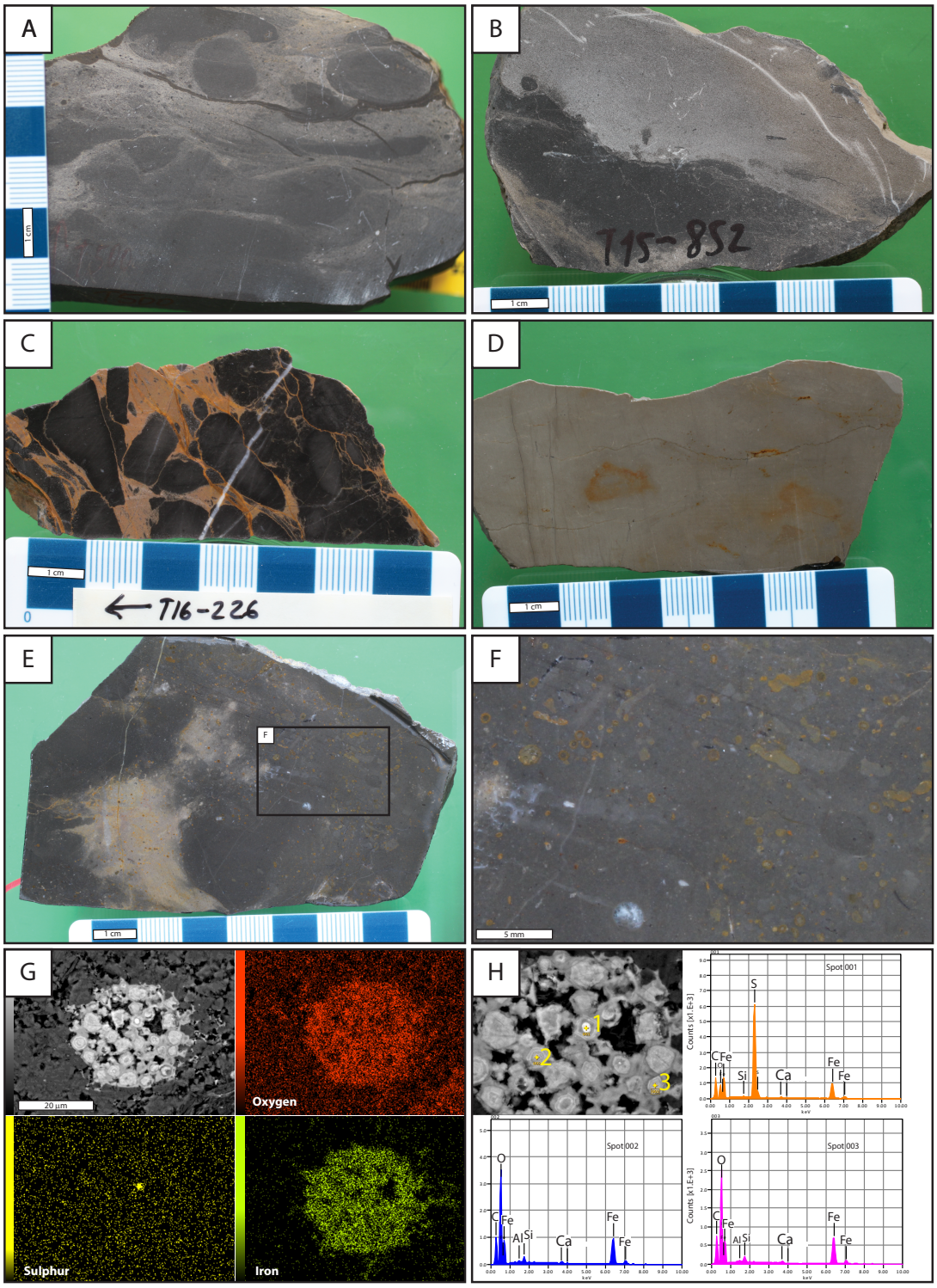
A
B
T15-852
C
T16-226
D
E
F
5 mm
G
20 µm
Oxygen
Sulphur
Iron
H
Spot 001
Spot 002
Spot 003
S
O
Fe
Si
Ca
Al

Figure 7

Figure 7 (previous page): Sedimentary features of the Bukovje spotted limestone facies. A) *Planolites*-burrowed mudstone. Darker regions are inferred to be more organic rich than lighter regions, which are likely more carbonate rich. B) Erosive contact between an organic-rich mudstone (bottom) and overlying carbonate grainflow deposit. C) Storm rip-up breccia in which the lithoclasts were once organic carbon-rich black shale. D) Organic poor, massive mudstone. E) Typical spotted limestone; organic-rich with pyrite framboids. F) Closeup of pyrite framboids in E. G) SEM and EDS maps of individual pyrite framboid, indicating that they have largely been oxidized to FeO minerals. H) EDS counts of individual crystals within the framboid. Only spot 1 still contains sulphur.

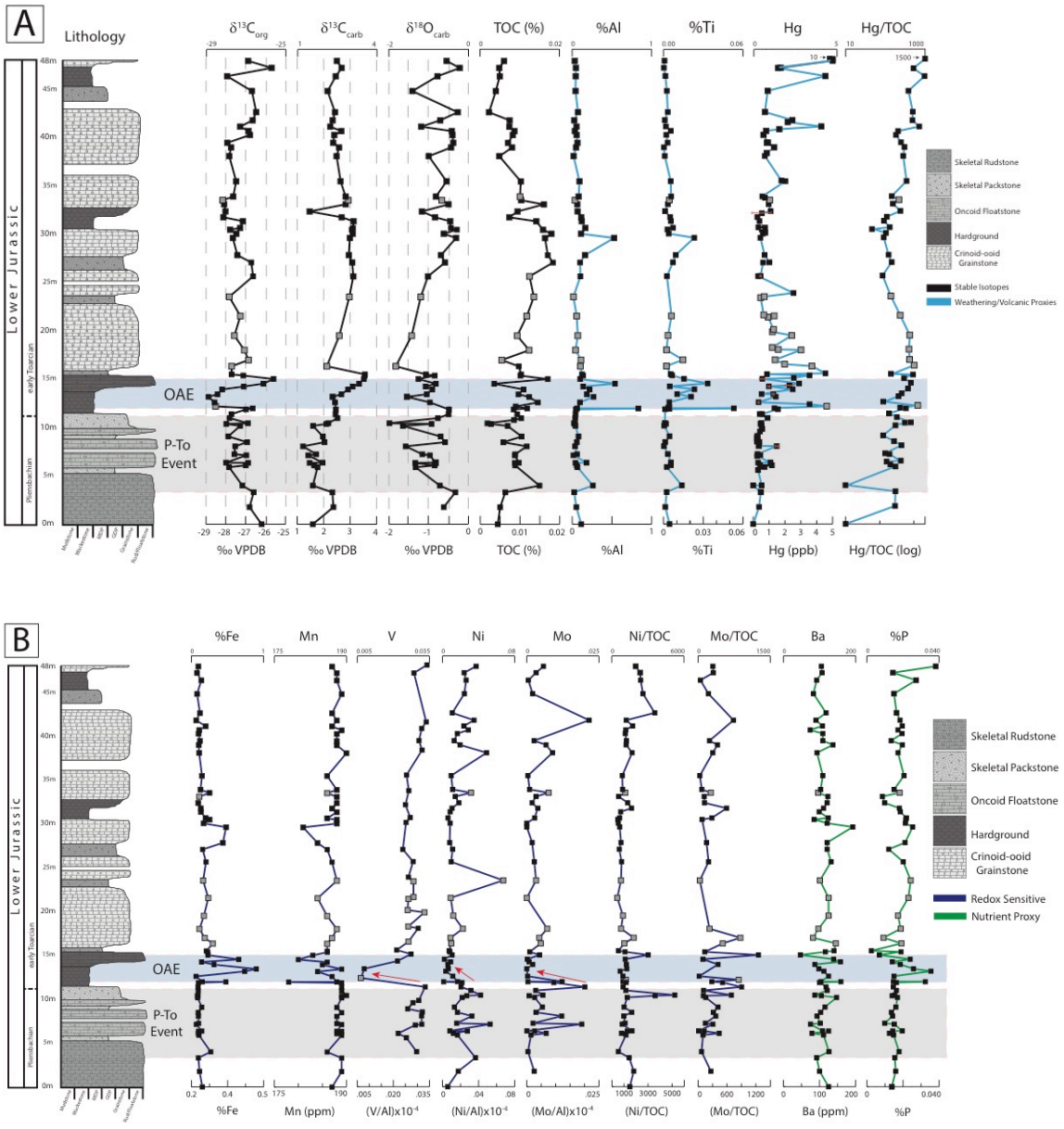

Figure 8: Chemostratigraphic results of the Kovk section. A) Stable isotope profiles (black) and weathering/volcanic element proxies (blue) (Al, Ti, Hg). B) Redox sensitive element profiles (purple) (Fe, Mn, V, Ni, Mo) and nutrient proxies (Ba, P). Grey data points represent samples with higher Mg/Ca ratios indicating partial dolomitization.

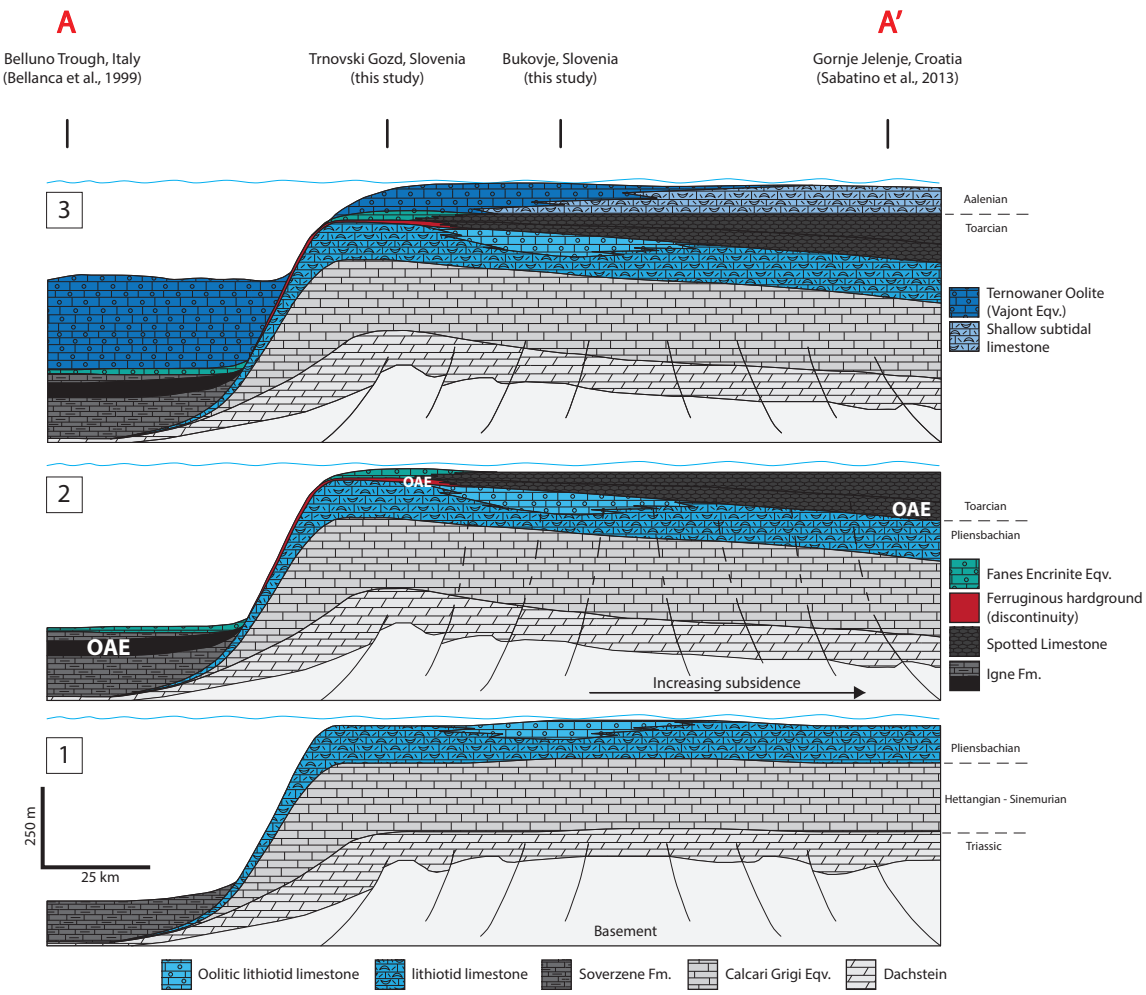
A
A'
Belluno Trough, Italy
(Bellanca et al., 1999)
Trnovski Gozd, Slovenia
(this study)
Bukovje, Slovenia
(this study)
Gornje Jelenje, Croatia
(Sabatino et al., 2013)
3
Aalenian
Toarcian
Ternowaner Oolite
(Vajont Eqv.)
Shallow subtidal
limestone
2
OAE
OAE
OAE
Toarcian
Pliensbachian
Fanes Encrinite Eqv.
Ferruginous hardground
(discontinuity)
Spotted Limestone
Igne Fm.
Increasing subsidence
1
Pliensbachian
Hettangian - Sinemurian
Triassic
250 m
25 km
Basement
Oolitic lithiotid limestone
lithiotid limestone
Soverzene Fm.
Calcari Grigi Eqv.
Dachstein

Figure 9

Figure 9 (previous page): Lower Jurassic evolution of the Adriatic Carbonate Platform; location of sections used can be found on figure 1 and formational equivalents in figure 11. Stage 1) Normal carbonate "keep-up" with widespread deposition of lithiotid limestone of the *Palaeodasycladus meditteraneus* biozone on a flat-topped platform. Stage 2) Onset of OAE yielding partial drowning of margin and development of discontinuity surface. Differential subsidence and restricted circulation yield a shallow ramp profile on the interior, and the deposition of the euxinic spotted limestone across SE Slovenia and Croatia. Black shale deposition occurs in adjacent Belluno Basin. The immediate aftermath of the OAE is characterized by oolitic-encrinitic shoals on the platform margin, whereas the interior continues to accumulate spotted limestones in an intrashelf basin. Stage 3) Amelioration of paleooceanographic conditions by the Middle Jurassic (Aalenian) results in the deposition of the Ternowaner oolite. The Ternowaner prograded toward the shelf interior, yielding the end of the spotted limestones, and into the Belluno Basin, yielding a thick westward prograding oolitic fan. A flat-topped platform was once again established.

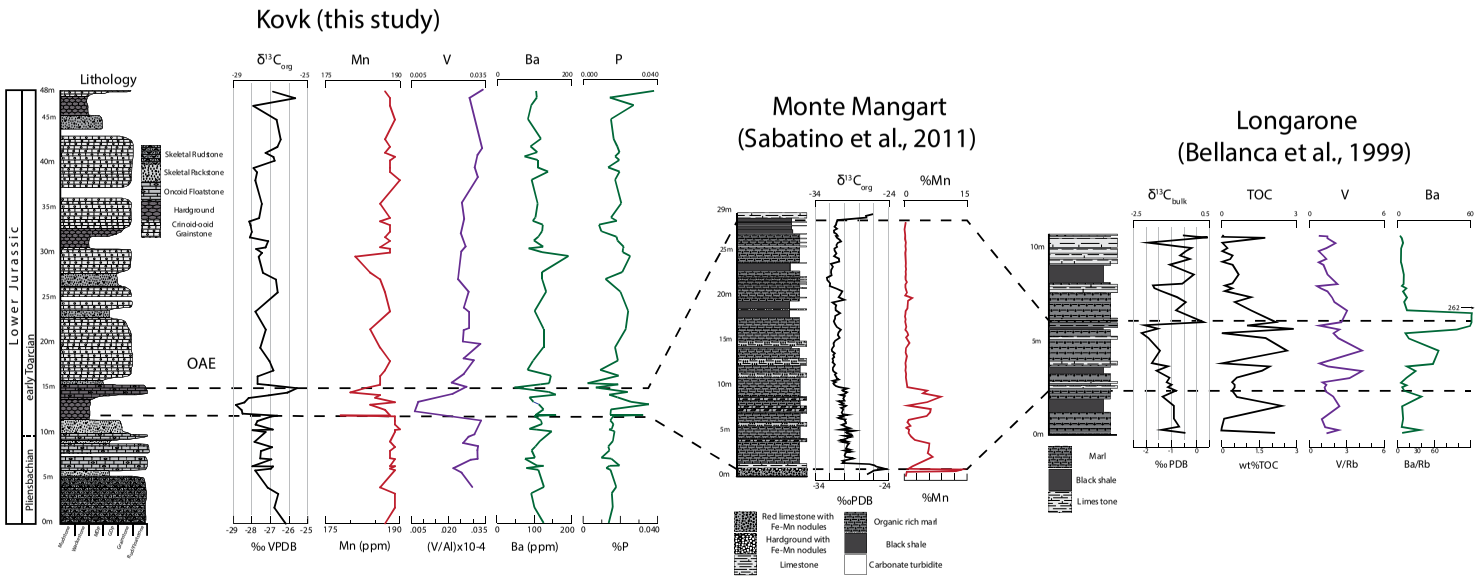

Figure 10: Chemostratigraphic correlation between the NW margin of the Adriatic Carbonate Platform and the adjacent Belluno and Julian basins. Elemental stratigraphy depicts reciprocal responses between sections that are discussed in the text. Paleogeographic location of sections can be found in Fig. 2. Note that sections are not illustrated at the same scale.

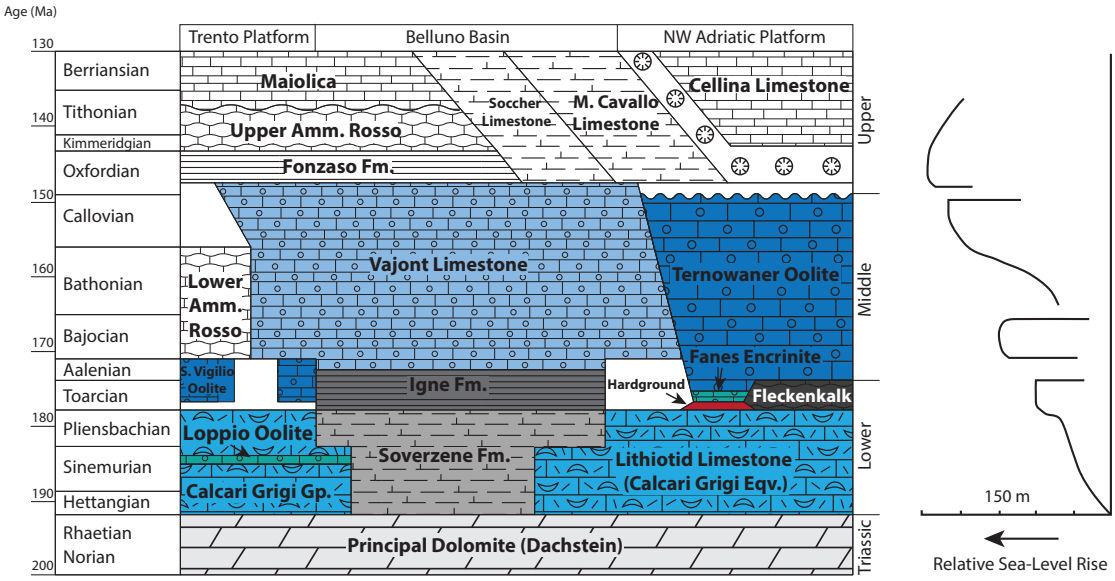

Figure 11: Chronostratigraphic chart of formations and lithofacies of the Adriatic Carbonate Platform and Adjacent Belluno Basin/Trento Platform. Modified from Bosellini et al. (1981) to include information from this study and that of Preto et al. (2017).

REFERENCES

Algeo, T. J. (2004). Can marine anoxic events draw down the trace element inventory of seawater? *Geology*, *32*(12), 1057–1060. http://doi.org/10.1130/G20896.1

Algeo, T. J., & Rowe, H. (2012). Paleoceanographic applications of trace-metal concentration data. *Chemical Geology*, *324–325*, 6–18. http://doi.org/10.1016/j.chemgeo.2011.09.002

Al-Suwaidi, A.H., Hesselbo, S.P., Damborenea, S.E., Manceñido, M.O., Jenkyns, H.C., Riccardi, A.C., Angelozzi, G.N., Baudin, F. (2016). The Toarican Oceanic Anoxic Event (Early Jurassic) in the Neuquén Basin, Argentina: a reassessment of age and carbon isotope stratigraphy. *The Journal of Geology, 124*, 171-193. http://doi.org/10.1086/684831

Bellanca, A., Masetti, D., Neri, R., & Venezia, F. (1999). Geochemical and sedimentological evidence of productivity cycles recorded in Toarcian black shales from the Belluno Basin, Southern Alps, northern Italy. *Journal of Sedimentary Research*, *69*(2), 466–476. http://doi.org/10.2110/jsr.69.466

Bodin, S., Krencker, F. N., Kothe, T., Hoffmann, R., Mattioli, E., Heimhofer, U., & Kabiri, L. (2016). Perturbation of the carbon cycle during the late Pliensbachian - early Toarcian: New insight from high-resolution carbon isotope records in Morocco. *Journal of African Earth Sciences*, *116* (October), 89–104. http://doi.org/10.1016/j.jafrearsci.2015.12.018

Bodin, S., Mattioli, E., Fröhlich, S., Marshall, J. D., Boutib, L., Lahsini, S., & Redfern, J. (2010). Toarcian carbon isotope shifts and nutrient changes from the Northern margin of Gondwana (High Atlas, Morocco, Jurassic): Palaeoenvironmental implications. *Palaeogeography, Palaeoclimatology, Palaeoecology*, *297*(2), 377–390. http://doi.org/10.1016/j.palaeo.2010.08.018

Boomer, I., Horne, D. J., & Slipper, I. J. (2003). The Use of Ostracods In Palaeoenvironmental Studies, Or What Can You Do With An Ostrocod Shell? *Paleontological Society Papers*, *9*, 153–180.

Boomer, I., & Whatley, R. (1992). Ostracoda and dysaerobia in the Lower Jurassic of Wales: the reconstruction of past oxygen levels. *Palaeogeography, Palaeoclimatology, Palaeoecology*, *99*(3–4), 373–379. http://doi.org/10.1016/0031-0182(92)90024-Y

Bosellini, A., Masetri, D., & Sarti, M. (1981). A Jurassic " Tongue of the Ocean " infilled with oolitic sands : The Belluno Trough, Venetian Alps. *Marine Geology, 44*, 59–95.

Bosscher, H., & Schlager, W. (1993). Accumulation Rates of Carbonate Platforms. *The Journal of Geology*, *101*(3), 345–355.

Boulila, S., Galbrun, B., Huret, E., Hinnov, L. A., Rouget, I., Gardin, S., & Bartolini, A. (2014). Astronomical calibration of the Toarcian Stage: Implications for sequence stratigraphy and duration of the early Toarcian OAE. *Earth and Planetary Science Letters*, *386*, 98–111. http://doi.org/10.1016/j.epsl.2013.10.047

Brand, U., & Veizer, J. (1981). Chemical diagenesis of a multicomponent carbonate system; 2, Stable isotopes. *Journal of Sedimentary Research*, *51*(3).

Brazier, J.-M., Suan, G., Tacail, T., Simon, L., Martin, J. E., Mattioli, E., & Balter, V. (2015). Calcium isotope evidence for dramatic increase of continental weathering during the Toarcian oceanic anoxic event (Early Jurassic). *Earth and Planetary Science Letters*, *411*, 164–176. http://doi.org/10.1016/j.epsl.2014.11.028

Burchette, T.P., Wright, V.P. (1992). Carbonate ramp depositional systems. In B.W. Sellwood (Ed.), *Ramps and Reefs* (Vol. 79, pp. 3-57). Sedimentary Geology.

Burdige, D. J. (1993). The biogeochemistry of manganese and iron reduction in marine sediments. *Earth-Science Reviews*, *35*, 249–284.

Burgess, S. D., Bowring, S. A., Fleming, T. H., & Elliot, D. H. (2015). High-precision geochronology links the Ferrar large igneous province with early-Jurassic ocean anoxia and biotic crisis. *Earth and Planetary Science Letters*, *415*, 90–99. http://doi.org/10.1016/j.epsl.2015.01.037

Čadjenović, D., Kilibarda, Z., & Radulović, N. (2008). Late Triassic to Late Jurassic evolution of the Adriatic Carbonate Platform and Budva Basin, Southern Montenegro. *Sedimentary Geology*, *204*(1–2), 1–17. http://doi.org/10.1016/j.sedgeo.2007.12.005

Caruthers, A. H., Smith, P. L., & Grocke, D. R. (2014). The Pliensbachian-Toarcian (Early Jurassic) extinction: A North American perspective. In *Geological Society of America Special Papers* (Vol. 505, pp. 225–243). Geological Society of America. http://doi.org/10.1130/2014.2505(11)

Caruthers, A. H., Smith, P. L., & Gröcke, D. R. (2013). The Pliensbachian-Toarcian (Early Jurassic) extinction, a global multi-phased event. *Palaeogeography, Palaeoclimatology, Palaeoecology*, *386*(November 2016), 104–118. http://doi.org/10.1016/j.palaeo.2013.05.010

Cohen, A. S., Coe, A. L., Harding, S. M., & Schwark, L. (2004). Osmium isotope evidence for the regulation of atmospheric CO2 by continental weathering. *Geology*, *32*(2), 157. http://doi.org/10.1130/G20158.1

Corbin, J.-C., Person, A., Iatzoura, A., Ferré, B., & Renard, M. (2000). Manganese in Pelagic carbonates: indication of major Tectonic events during the geodynamic evolution of a passive continental margin (the Jurassic European Margin of the Tethys–Ligurian Sea). *Palaeogeography, Palaeoclimatology, Palaeoecology*, *156*, 123–138.

Črne, A. E. (2009). Depositional Model of Lower Jr. Carbonates on the Dinaric Carbonate Platform Margin. *Unpublished Doctoral Dissertation, UNIVERZA V LJUBLJANI, Ljubljana, Slovenia*.

Črne, A. E., & Goričan, S. (2008). The Dinaric Carbonate Platform margin in the Early Jurassic: a comparison between successions in Slovenia and Montenegro. *Bollettino Societa' Geologica Italiana*, *127*(2), 389–405.

Danise, S., Twitchett, R. J., Little, C. T. S., & Clemence, M. E. (2013). The impact of global warming and anoxia on marine benthic community dynamics: an example from the Toarcian (Early Jurassic). *Plos One*, *8*(2), e56255. http://doi.org/10.1371/journal.pone.0056255

Debeljak, I., Buser, S. (1997). Middle Liassic-Lower bivalves in Slovenia and their model of life.

Geologija, 40, 11-64.

De Castro, P. (1962). Nuove osservazioni sul livello ad Orbitolina in Campania (Nota preliminare). *Bollettino della Societa` dei Naturalisti in Napoli, 71,* 103–135.

De Castro, P. (1963). Cuneolina scarsellai n. sp. Nel Cretacico dell'Appennino meridionale. *Bollettino della Societa` dei Naturalisti in Napoli, 72*, 71–76.

De Keyser, T. L., & Kendall, C. G. (2014). Jurassic and Cretaceous sedimentary fill of intrashelf basins of the eastern margin the Arabian Plate, *30322*.

Degens, E. T., Guillard, R. R. L., Sackett, W. M., & Hellebust, J. A. (1968). Metabolic fractionation of carbon isotopes in marine plankton—I. Temperature and respiration experiments. *Deep Sea Research and Oceanographic Abstracts*, *15*(1), 1–9. http://doi.org/10.1016/0011-7471(68)90024-7

Demicco, R. V., Lowenstein, T. K., Hardie, L. A., & Spencer, R. J. (2005). Model of seawater composition for the Phanerozoic. *Geology*, *33*(11), 877. http://doi.org/10.1130/G21945.1

Dickson, J. A. D. (1966). Carbonate identification and genesis as revealed by staining. *Journal of Sedimentary Petrology*, *36*(2), 491–505.

Dickson, J. A. D., & Coleman, M. L. (1980). Changes in carbon and oxygen isotope composition during limestone diagenesis. *Sedimentology*, *27*(1), 107–118. http://doi.org/10.1111/j.1365-3091.1980.tb01161.x

Dozet, S. (1997). Biostratigraphy of shallow marine Jurassic beds in southeastern Slovenia. *Geologija*. http://doi.org/10.5474/geologija.1997.008

Dumas, S., & Arnott, R. W. C. (2006). Origin of hummocky and swaley cross-stratification— The controlling influence of unidirectional current strength and aggradation rate. *Geology*, *341*(4), 1073–1076. http://doi.org/10.1130/G22930A.1

Elliott, G. F. (1968). Ecologic significance of post-Palaeozoic green calcareous algae. *Geol. Mag.*, *115*, 437–442. http://doi.org/10.1017/S001675680004173X

Elliott, G. F. (1991). Dasycladalean Algae of the Palaeozoic and Mesozoic. In R. Riding (Ed.), *Calcareous Algae and Stromatolites* (pp. 125–130). Berlin, Heidelberg: Springer Berlin Heidelberg. http://doi.org/10.1007/978-3-642-52335-9_7

Embry, A.F., Klovan, E.J. (1971). A Late Devonian reef tract on northeastern Banks Island, N.W.T.: *Bulletin of Canadian Petroleum Geology, 19*, 730-781.

Emerson, S. R., & Huested, S. S. (1991). Ocean anoxia and the concentrations of molybdenum and vanadium in seawater. *Marine Chemistry*, *34*(3–4), 177–196. http://doi.org/10.1016/0304-4203(91)90002-E

Evamy, B. D. (1969). The Precipitational Environment and Correlation of Some Calcite Cements Deduced from Artificial Staining. *Journal of Sedimentary Petrology*, *39*(2), 787–821.

Farinacci, A. & Radoičić, R. (1964). Correlazioni fra le serie giuresi e cretacee dell'Apennino Centrale e delle Dinaridi Esterne. *Ricerca Sci. (Rendiconti), 34,* 269–300.

Fischer, A. G. (1975). Tidal deposits, Dachstein Limestone of the North-Alpine Triassic, In Ginsburg, R. N., (Ed.), *Tidal deposits* (pp. 235-242). *New York, Springer-Verlag*.

Force, E. R., & Cannon, W. F. (1988). Depositional Model for Shallow-Marine Manganese Deposits around Black Shale Basins. *Economic Geology*, *83*, 93–117. Retrieved from http://econgeol.geoscienceworld.org/content/econgeo/83/1/93.full.pdf

French, K. L., Sepúlveda, J., Trabucho-Alexandre, J., Gröcke, D. R., & Summons, R. E. (2014). Organic geochemistry of the early Toarcian oceanic anoxic event in Hawsker Bottoms, Yorkshire, England. *Earth and Planetary Science Letters*, *390*, 116–127. http://doi.org/10.1016/j.epsl.2013.12.033

Froelich, P. N., Klinkhammer, G. P., Bender, M. L., Luedtke, N. A., Heath, G. R., Cullen, D., Maynard, V. (n.d.). Early oxidation of organic matter in pelagic sediments of the eastern equatorial Atlantic: suboxic diagenesis. *Geochimica et Cosmochimica Acta, 43*(7), 1075-1090.

Fry, B., Jannasch, H. W., Molyneaux, S. J., Wirsen, C. O., Muramoto, J. A., & King, S. (1991). Stable isotope studies of the carbon, nitrogen and sulfur cycles in the Black Sea and the Cariaco Trench. *Deep Sea Research Part A. Oceanographic Research Papers*, *38*, S1003–S1019. http://doi.org/10.1016/S0198-0149(10)80021-4

Gale, L. (2014). Lower Jurassic foraminiferal biostratigraphy of Podpeč Limestone (External Dinarides, Slovenia). *Geologija*, *57*(2), 119–146. http://doi.org/10.5474/geologija.2014.011

Gill, B. C., Lyons, T. W., & Jenkyns, H. C. (2011). A global perturbation to the sulfur cycle during the Toarcian Oceanic Anoxic Event. *Earth and Planetary Science Letters*, *312*(3–4), 484–496. http://doi.org/10.1016/j.epsl.2011.10.030

Goldhammer, R. K., Dunn, P. A., & Hardie, L. A. (1990). Depositional cycles, composite sea-level changes, cycle stacking patterns, and the hierarchy of stratigraphic forcing: Examples from Alpine Triassic platform carbonates. *Bulletin of the Geological Society of America*, *102*(5), 535–562. http://doi.org/10.1130/0016-7606(1990)102<0535:DCCSLC>2.3.CO;2

Grasby, S. E., Beauchamp, B., Bond, D. P. G., Wignall, P. B., & Sanei, H. (2016). Mercury anomalies associated with three extinction events (Capitanian Crisis, Latest Permian Extinction and the Smithian/Spathian Extinction) in NW Pangea. *Geol. Mag*, *153*(2), 285–297. http://doi.org/10.1017/S0016756815000436

Graziano, R. (1999). The Early Cretaceous drowning unconformities of the Apulia carbonate platform (Gargano Promontory, southern Italy): local fingerprints of global palaeoceanographic events. *Terra Nova*, *11*(6), 245–250. http://doi.org/10.1046/j.1365-3121.1999.00256.x

Graziano, R., Buono, G., & Ruggiero, E. (2006). Lower Toarcian (Jurassic) brachiopod-rich carbonate facies of the Gran Sasso range (central Apennines, Italy). *Bollettino Della Societa Paleontologica Italiana*, *45*(1), 61–74.

Greene, S. E., Martindale, R. C., Ritterbush, K. A., Bottjer, D. J., Corsetti, F. A., & Berelson, W. M. (2012). Recognising ocean acidification in deep time: An evaluation of the evidence for acidification across the Triassic-Jurassic boundary. *Earth-Science Reviews*, *113*(1), 72–93. http://doi.org/10.1016/j.earscirev.2012.03.009

Gröcke, D. R., Hori, R. S., Trabucho-Alexandre, J., Kemp, D. B., & Schwark, L. (2011). An open ocean record of the Toarcian oceanic anoxic event. *Solid Earth*, *2*, 245–257. http://doi.org/10.5194/se-2-245-2011

Grossman, E. L., & Ku, T. (1986). Oxygen and carbon isotope fractionation in biogenic aragonite: Temperature effects - ScienceDirect. *Chemical Geology: Isotope Geoscience Section*, *59*, 59–74.

Groves, J. R., & Calner, M. (2004). Lower Triassic oolites in Tethys: A sedimentologic response to the end-Permian mass extinction (abs.): *Geological Society of America Annual Meeting, Abstracts with Program, 36*(5), 336.

Hallam, A. (1981). A revised sea-level curve for the early Jurassic. *J. Geol. Soc. London*, *138*, 735–743. Retrieved from http://jgs.lyellcollection.org/content/138/6/735.full.pdf

Hardenbol, J., Thierry, J., Farley, M. B., Jacquin, T., De Graciansky, P.-C., & Vail, P. R. (1998). Mesozoic And Cenozoic sequence chronostratigraphic framework of European basins. In P.-C. de Graciansky, J. Hardenbol, T. Jacquin, & P. R. Vail (Eds.), *Mesozoic and Cenozoic Sequence Stratigraphy of European Basins, Special Publication* (60th ed., pp. 3–13). Society for Sedimentary Geology.

Hermoso, M., Minoletti, F., Le Callonnec, L., Jenkyns, H. C., Hesselbo, S. P., Rickaby, R. E. M., Emmanuel, L. (2009). Global and local forcing of Early Toarcian seawater chemistry: A comparative study of different paleoceanographic settings (Paris and Lusitanian basins). *Paleoceanography*, *24*(4). http://doi.org/10.1029/2009PA001764

Hermoso, M., Minoletti, F., Rickaby, R. E. M., Hesselbo, S. P., Baudin, F., & Jenkyns, H. C. (2012). Dynamics of a stepped carbon-isotope excursion: Ultra high-resolution study of Early Toarcian environmental change. *Earth and Planetary Science Letters*, *319–320*, 45–54. http://doi.org/10.1016/j.epsl.2011.12.021

Hesselbo, S. P., Gröcke, D. R., Jenkyns, H. C., Bjerrum, C. J., Farrimond, P., Morgans Bell, H. S., & Green, O. R. (2000). Massive dissociation of gas hydrate during a Jurassic oceanic anoxic event. *Nature*, *406*(6794), 392–395. http://doi.org/10.1038/35019044

Hesselbo, S. P., Jenkyns, H. C., Duarte, L. V., & Oliveira, L. C. V. (2007). Carbon-isotope record of the Early Jurassic (Toarcian) Oceanic Anoxic Event from fossil wood and marine carbonate (Lusitanian Basin, Portugal). *Earth and Planetary Science Letters*, *253*(3–4), 455–470. http://doi.org/10.1016/j.epsl.2006.11.009

Honisch, B., Ridgwell, A., Schmidt, D. N., Thomas, E., Gibbs, S. J., Sluijs, A., Williams, B. (2012). The Geological Record of Ocean Acidification. *Science*, *335*(6072), 1058–1063.

Horne, D. J., Brandão, S. N., & Slipper, I. J. (2011). The Platycopid Signal deciphered: Responses of ostracod taxa to environmental change during the Cenomanian–Turonian Boundary Event (Late Cretaceous) in SE England. *Palaeogeography, Palaeoclimatology, Palaeoecology*, *308*(3), 304–312. http://doi.org/10.1016/j.palaeo.2011.05.034

Ikeda, M., & Hori, R. S. (2014). Effects of Karoo–Ferrar volcanism and astronomical cycles on the Toarcian oceanic anoxic events (Early Jurassic). *Palaeogeography, Palaeoclimatology, Palaeoecology*, *410*, 134–142. http://doi.org/10.1016/j.palaeo.2014.05.026

Jenkyns, H. C. (2010). Geochemistry of oceanic anoxic events. *Geochemistry, Geophysics, Geosystems*, *11*(3), Q03004. http://doi.org/10.1029/2009GC002788

Jenkyns, H. C., & Clayton, C. J. (1997). Lower Jurassic epicontinental carbonates and mudstones from England and Wales: chemostratigraphic signals and the early Toarcian anoxic event. *Sedimentology*, *44*, 687–706.

Jenkyns, H. C., Sarti, M., Masetti, D., & Howarth, M. K. (1985). Ammonites and stratigraphy of Lower Jurassic black shales and pelagic limestones from Belluno Trough, Trough Alps, Italy. *Eclogae Geol. Helv.*, *78*.

Kemp, D. B., Coe, A. L., Cohen, A. S., & Schwark, L. (2005). Astronomical pacing of methane release in the Early Jurassic period. *Nature*, *437*(7057), 396–399. http://doi.org/10.1038/nature04037

Kerans, C., Fitchen, W.M., 1995. Sequence stratigraphy and facies architecture of a carbonate ramp system: San Andres Formation of Algerita escarpment and western Guadalupe Mountains, West Texas and New Mexico. *Bureau of Economic Geology, University of Texas at Austin, Report of Investigations 235*.

Korbar, T. (2009). Orogenic evolution of the External Dinarides in the NE Adriatic region: a model constrained by tectonostratigraphy of Upper Cretaceous to Paleogene carbonates. *Earth-Science Reviews*, *96*(4), 296–312. http://doi.org/10.1016/j.earscirev.2009.07.004

Kossmat, F., 1905. Erl uterung zur geologischen Karte der Osterreich-Ungar Monarchie, SW-Gruppe, 98: Heidenschaft und Adelsberg. K.K. *Geol. Reichanst., Wien*.

Krencker, F. N., Bodin, S., Suan, G., Heimhofer, U., Kabiri, L., & Immenhauser, A. (2015). Toarcian extreme warmth led to tropical cyclone intensification. *Earth and Planetary Science Letters*, *425*, 120–130. http://doi.org/10.1016/j.epsl.2015.06.003

Kump, L. R., & Arthur, M. a. (1999). Interpreting carbon-isotope excursions: carbonates and organic matter. *Chemical Geology*, *161*(1–3), 181–198. http://doi.org/10.1016/S0009-2541(99)00086-8

Kump, L. R., Bralowe, T. J., & Ridgwell, A. (2009). Ocean Acidification in Deep Time. *Oceanography*, *22*(4), 94–107. http://doi.org/10.5670/oceanog.2009.100

Kuroda, J., Ogawa, N. O., Tanimizu, M., Coffin, M. F., Tokuyama, H., Kitazato, H., & Ohkouchi, N. (2007). *Contemporaneous massive subaerial volcanism and late cretaceous Oceanic Anoxic Event 2. Earth and Planetary Science Letters* (Vol. 256).

Larson, R. L., & Erba, E. (1999). Onset of the Mid-Cretaceous greenhouse in the Barremian-Aptian: Igneous events and the biological, sedimentary, and geochemical responses. *Paleoceanography*, *14*(6), 663–678. http://doi.org/10.1029/1999PA900040

Lehrmann, D. J., Minzoni, M., Li, X., Yu, M., Payne, J. L., Kelley, B. M., Payne, J. (2012). Lower Triassic oolites of the Nanpanjiang Basin, south China: Facies architecture, giant ooids, and diagenesis—Implications for hydrocarbon reservoirs. *AAPG Bulletin*, *96*(8), 1389–1414. http://doi.org/10.1306/01231211148

Léonide, P., Floquet, M., Durlet, C., Baudin, F., Pittet, B., & Lécuyer, C. (2012). Drowning of a carbonate platform as a precursor stage of the Early Toarcian global anoxic event (Southern Provence sub-Basin, South-east France). *Sedimentology*, *59*(1), 156–184. http://doi.org/10.1111/J.1365-3091.2010.01221.X

Littler, K., Hesselbo, S. P., & Jenkyns, H. C. (2010). A carbon-isotope perturbation at the Pliensbachian–Toarcian boundary: evidence from the Lias Group, NE England. *Geological Magazine*, *147*(2), 181. http://doi.org/10.1017/S0016756809990458

Lu, Z., Jenkyns, H. C., & Rickaby, R. E. . (2010). You have access Iodine to calcium ratios in marine carbonate as a paleo-redox proxy during oceanic anoxic events. *Geology*, *38*(12), 1107–1110. http://doi.org/10.1130/G31145.1

Lyons, T. W., Anbar, A. D., Severmann, S., Scott, C., & Gill, B. C. (2009). Tracking Euxinia in the Ancient Ocean: A Multiproxy Perspective and Proterozoic Case Study. *Annual Review of Earth and Planetary Sciences*, *37*(1), 507–534. http://doi.org/10.1146/annurev.earth.36.031207.124233

Lyons, T. W., Reinhard, C. T., & Planavsky, N. J. (2014). The rise of oxygen in Earth's early ocean and atmosphere. *Nature*, *506*(7488), 307–15. http://doi.org/10.1038/nature13068

Martindale, R.C., Aberhan, M. (*in press*). Response of macrobenthic communities to the Toarcian Oceanic Anoxic Event in northeastern Panthalassa (Ya Ha Tinda, Alberta, Canada). *Palaeogeography, Palaeoclimatology, Palaeoecology*. http://dx.doi.org/10.1016/j.palaeo.2017.01.009

Masetti, D., Bottoni, A., 1978. L'Encrinite di Fanes e suo inquadrarnento nella paleogeografia giurassica dell'area Dolomitica. *Riv. Ital. Paleontol. Stratigr., 84*, 169-186.

Mallarino, G., Goldstein, R. H., & Di Stefano, P. (2002). New approach for quantifying water depth applied to the enigma of drowning of carbonate platforms. *Geology*, *30*(4), 783–786. Retrieved from http://geology.geoscienceworld.org/content/geology/30/9/783.full.pdf

Marshall, J. D. (1992). Climatic and oceanographic isotopic signals from the carbonate rock record and their preservation. *Geol. Mag*, *129*(2), 143–160. http://doi.org/10.1017/S0016756800008244

Mattioli, E., Pittet, B., Palliani, R., ROhl, H.-J., Schmid-ROhl, a., & Morettini, E. (2004). Phytoplankton evidence for the timing and correlation of palaeoceanographical changes during the early Toarcian oceanic anoxic event (Early Jurassic). *Journal of the Geological Society*, *161*(4), 685–693. http://doi.org/10.1144/0016-764903-074

McElwain, J. C., Wade-Murphy, J., & Hesselbo, S. P. (2005). Changes in carbon dioxide during an oceanic anoxic event linked to intrusion into Gondwana coals. *Nature*, *435*(7041), 479–482. http://doi.org/10.1038/nature03618

Milliman, J.D. (1974). Recent sedimentary carbonates: part 1. Marine carbonates. *Springer- Verlag, Berlin Heidelberg New York*.

Montero-Serrano, J.-C., Föllmi, K. B., Adatte, T., Spangenberg, J. E., Tribovillard, N., Fantasia, A., & Suan, G. (2015). Continental weathering and redox conditions during the early Toarcian Oceanic Anoxic Event in the northwestern Tethys: Insight from the Posidonia Shale section in the Swiss Jura Mountains. *Palaeogeography, Palaeoclimatology, Palaeoecology*, *429*, 83–99. http://doi.org/10.1016/j.palaeo.2015.03.043

Mucci, A. (1983). The solubility of calcite and aragonite in seawater at various salinities, temperatures, and one atmosphere total pressure, *American Journal of Science, 283*, 780–799.

Müller, T., Price, G. D., Bajnai, D., Nyerges, A., Kesjár, D., Raucsik, B., Pálfy, J. (2017). New multiproxy record of the Jenkyns Event (also known as the Toarcian Oceanic Anoxic Event) from the Mecsek Mountains (Hungary): Differences, duration and drivers. *Sedimentology*, *64*(1), 66–86. http://doi.org/10.1111/sed.12332

Opdyke, B.N., Wilkinson, B.H. (1990). Paleolatitude distribution of Phanerozoic marine ooids and cements, *Palaeogeography, Palaeoclimatology, Palaeoecology*, *78*, 135-148.

Owens, J. D., Reinhard, C. T., Rohrssen, M., Love, G. D., & Lyons, T. W. (2016). Empirical links between trace metal cycling and marine microbial ecology during a large perturbation to Earth's carbon cycle. *Earth and Planetary Science Letters*, *449*, 407–417. http://doi.org/10.1016/j.epsl.2016.05.046

Pálfy, J., & Smith, P. L. (2000). Synchrony between Early Jurassic extinction, oceanic anoxic event, and the Karoo-Ferrar flood basalt volcanism. *Geology*, *28*(8), 747–750. http://doi.org/10.1130/0091-7613(2000)28<747:SBEJEO>2.0.CO

Payne, J. L., Lehrmann, D. J., Wei, J., & Knoll, A. H. (2006). The pattern and timing of biotic recovery from the End-Permian Extinction on the Great Bank of Guizhou, Guizhou Province, China. *Palaios*, *21*(1), 63–85. http://doi.org/10.2110/palo.2005.p05-12p

Percival, L. M. E., Cohen, A. S., Davies, M. K., Dickson, A. J., Hesselbo, S. P., Jenkyns, H. C., Xu, W. (2016). Osmium isotope evidence for two pulses of increased continental weathering linked to Early Jurassic volcanism and climate change. *Geology*, *44*(9), 759–762. http://doi.org/10.1130/G37997.1

Percival, L. M. E., Witt, M. L. I., Mather, T. A., Hermoso, M., Jenkyns, H. C., Hesselbo, S. P., Ruhl, M. (2015). Globally enhanced mercury deposition during the end-

Pliensbachian extinction and Toarcian OAE: A link to the Karoo–Ferrar Large Igneous Province. *Earth and Planetary Science Letters*, *428*, 267–280. http://doi.org/10.1016/j.epsl.2015.06.064

Phelps, R. M., Kerans, C., Da-Gama, R. O. B. P., Jeremiah, J., Hull, D., & Loucks, R. G. (2015). Response and recovery of the Comanche carbonate platform surrounding multiple Cretaceous oceanic anoxic events, northern Gulf of Mexico. *Cretaceous Research*, *54*, 117–144. http://doi.org/10.1016/j.cretres.2014.09.002

Phelps, R. M., Kerans, C., Loucks, R. G., Da Gama, R. O. B. P., Jeremiah, J., & Hull, D. (2014). Oceanographic and eustatic control of carbonate platform evolution and sequence stratigraphy on the Cretaceous (Valanginian-Campanian) passive margin, northern Gulf of Mexico. *Sedimentology*, *61*(2), 461–496. http://doi.org/10.1111/sed.12062

Pieńkowski, G., Hodbod, M., & Ullmann, C. V. (2016). Fungal decomposition of terrestrial organic matter accelerated Early Jurassic climate warming. *Scientific Reports*, *6*, 31930. http://doi.org/10.1038/srep31930

Placer, L., Vrabec, M., & Celarc, B. (2010). The bases for understanding of the NW Dinarides and Istria Peninsula tectonics. *Geologija*, *53*(1), 55–86. http://doi.org/doi:10.5474/geologija.2010.005

Posenato, R., & Masetti, D. (2012). Environmental control and dynamics of Lower Jurassic bivalve build-ups in the Trento Platform (Southern Alps, Italy). *Palaeogeography, Palaeoclimatology, Palaeoecology*, *361–362*, 1–13. http://doi.org/10.1016/j.palaeo.2012.07.001

Preto, N., Breda, A., Dal Corso, J., Franceschi, M., Rocca, F., Spada, C., & Roghi, G. (2017). The Loppio Oolitic Limestone (Early Jurassic, Southern Alps): A prograding oolitic body with high original porosity originated by a carbonate platform crisis and recovery. *Marine and Petroleum Geology*, *79*, 394–411. http://doi.org/10.1016/j.marpetgeo.2016.10.027

Pruss, S. B., Bottjer, D. J., Corsetti, F. A., & Baud, A. (2006). A global marine sedimentary response to the end-Permian mass extinction: Examples from southern Turkey and the western United States. *Earth-Science Reviews*, *78*(3), 193–206. http://doi.org/10.1016/j.earscirev.2006.05.002

Pyle, D. M., & Mather, T. A. (2003). The importance of volcanic emissions for the global atmospheric mercury cycle. *Atmospheric Environment*, *37*(36), 5115–5124. http://doi.org/10.1016/j.atmosenv.2003.07.011

Read, F. J. (1985). Carbonate Platform Facies Models. *AAPG Bulletin*, *69*(1), 1–21.

Ridgwell, A., & Zeebe, R. (2005). The role of the global carbonate cycle in the regulation and evolution of the Earth system. *Earth and Planetary Science Letters*, *234*(3–4), 299–315. http://doi.org/10.1016/j.epsl.2005.03.006

Rowe, H., Hughes, N., & Robinson, K. (2012). The quantification and application of handheld energy-dispersive x-ray fluorescence (ED-XRF) in mudrock chemostratigraphy and geochemistry. *Chemical Geology*, *324–325*, 122–131. http://doi.org/10.1016/j.chemgeo.2011.12.023

Sabatino, N., Neri, R., Bellanca, A., Jenkyns, H. C., Baudin, F., Parisi, G., & Masetti, D. (2009). Carbon-isotope records of the Early Jurassic (Toarcian) oceanic anoxic event from the Valdorbia (Umbria-Marche Apennines) and Monte Mangart (Julian Alps) sections: Palaeoceanographic and stratigraphic implications. *Sedimentology*, *56*(5), 1307–1328. http://doi.org/10.1111/j.1365-3091.2008.01035.x

Sabatino, N., Neri, R., Bellanca, A., Jenkyns, H. C., Masetti, D., & Scopelliti, G. (2011). Petrography and high-resolution geochemical records of Lower Jurassic manganese-rich deposits from Monte Mangart, Julian Alps. *Palaeogeography, Palaeoclimatology, Palaeoecology*, *299*(1–2), 97–109. http://doi.org/10.1016/j.palaeo.2010.10.039

Sabatino, N., Vlahovic¨, I., Jenkyns, H. C., Scopelliti, G., Neri, R., Prtoljan, B., & Velic¨, I. (2013). Carbon-isotope record and palaeoenvironmental changes during the early toarcian oceanic anoxic event in shallow-marine carbonates of the adriatic carbonate platform in Croatia. *Geological Magazine*, *150*, 1085–1102. http://doi.org/10.1017/S0016756813000083

Sandberg, P. A. (1983). An oscillating trend in Phanerozoic non-skeletal carbonate mineralogy. *Nature*, *305*(5929), 19–22. http://doi.org/10.1038/305019a0

Sanei, H., Grasby, S. E., & Beauchamp, B. (2012). Latest Permian mercury anomalies. *Geology*, *40*(1), 63–66. http://doi.org/10.1130/G32596.1

Sartoni S. & Crescenti U. (1961) - Ricerche biostratigrafiche nel Mesozoico dell'Appennino meridionale. *G. Geol., 29*, 161- 302.

Schlager, W. (1989). Drowning Unconformities on Carbonate Platforms. In P. D. Crevello, J. L. Wilson, J. F. Sarg, & J. F. Read (Eds.), *Controls on Carbonate Platform and Basin Development* (pp. 15–25). The Society of Economic Paleontologists and Mineralogists.

Schlager, W. (1981). The paradox of drowned reefs and carbonate platforms. *Geological Society of America Bulletin*, *92*(4), 197. http://doi.org/10.1130/0016-7606(1981)92<197:TPODRA>2.0.CO;2

Schlager, W. (2003). Benthic carbonate factories of the Phanerozoic. *International Journal of Earth Sciences, 92*(4), 445-464. http://doi.org/10.1007/s00531-003-0327-x

Schouten, S., Van Kaam-Peters, H. M. E., Irene, W., Rijpstra, C., Schoell, M., & Sinninghe Damste, J. S. (2000). Effects of an oceanic anoxic event on the stable

carbon isotopic composition of early Toarcian carbon. *American Journal of Science*, *300*, 1–22.

Septfontaine, M., Arnaud-Vanneau, A., Bassoullet, J.-P., Gusic, Y., Ramalho, M., Velic, I. (1991). Foraminifera of Jurassic shallow-water carbonate platforms: state of knowledge and future prospects. *Bulletin de la Société vaudoise des sciences naturelles, 80*(3), 255-277.

Sial, A. N., Lacerda, L. D., Ferreira, V. P., Frei, R., Marquillas, R. A., Barbosa, J. A., Pereira, N. S. (2013). Mercury as a proxy for volcanic activity during extreme environmental turnover: The Cretaceous–Paleogene transition. *Palaeogeography, Palaeoclimatology Palaeoecology*, *387*, 153–164. http://doi.org/10.1016/j.palaeo.2013.07.019

Sinton, C. W., & Duncan, R. A. (1997). Potential links between ocean plateau volcanism and global ocean anoxia at the Cenomanian-Turonian boundary. *Economic Geology*, *92*(7–8), 836–842. http://doi.org/10.2113/gsecongeo.92.7-8.836

Sitgreaves, J. R. (2015). Shelf-To-Basin Architecture And Facies Variability Of A Cretaceous Intrashelf Basin In The Northwest Gulf Of Mexico. *Unpublished Master's Thesis, The University of Texas at Austin*.

Smuc, A., & Gorican, S. (2005). Jurassic Sedimentary Evolution of a Carbonate Platform into a Deep-Water Basin, Mt. Mangart (Slovenian-Italian Border), *111*(1), 45–70.

Snedden, J.W., Nummedal, D., & Amos, A. F. (1988). Storm- and Fair-Weather Combined Flow on the Central Texas Continental Shelf. *SEPM Journal of Sedimentary Research*, *Vol. 58*(4), 580–595. http://doi.org/10.1306/212F8DFA-2B24-11D7-8648000102C1865D

Stanley, S. M., & Hardie, L. A. (1998). Secular oscillations in the carbonate mineralogy of reef-building and sediment-producing organisms driven by tectonically forced shifts in seawater chemistry. *Palaeogeography, Palaeoclimatology, Palaeoecology*, *144*(1–2), 3–19. http://doi.org/10.1016/S0031-0182(98)00109-6

Stanley, S. M., Ries, J. B., & Hardie, L. A. (2010). Increased Production of Calcite and Slower Growth for the Major Sediment-Producing Alga Halimeda as the Mg/Ca Ratio of Seawater is Lowered. *Journal of Sedimentary Research*, *80*(1), 6–16. http://doi.org/10.2110/jsr.2010.011

Steinthorsdottir, M., & Vajda, V. (2015). Early Jurassic (late Pliensbachian) CO_2 concentrations based on stomatal analysis of fossil conifer leaves from eastern Australia. *Gondwana Research*, *27*(3), 932–939. http://doi.org/10.1016/j.gr.2013.08.021

Suan, G., Mattioli, E., & Pittet, B. (2008). Evidence for major environmental perturbation prior to and during the Toarcian (Early Jurassic) oceanic anoxic event from the Lusitanian Basin, Portugal. *Paleoceanography, 23*(PA1202), 14. http://doi.org/10.1029/2007PA001459

Suan, G., Mattioli, E., Pittet, B., Lécuyer, C., Suchéras-Marx, B., Duarte, L. V., Martineau, F. (2010). Secular environmental precursors to Early Toarcian (Jurassic) extreme climate changes. *Earth and Planetary Science Letters, 290*(3), 448-458.

Suan, G., Schlögl, J., & Mattioli, E. (2016). Bio- and chemostratigraphy of the Toarcian organic-rich deposits of some key successions of the Alpine Tethys. *Newsletters on Stratigraphy*, *49*(3), 401–419. http://doi.org/10.1127/nos/2016/0078

Suan, G., van de Schootbrugge, B., Adatte, T., Fiebig, J., & Oschmann, W. (2015). Calibrating the magnitude of the Toarcian carbon cycle perturbation. *Paleoceanography*, *30*(5), 495–509. http://doi.org/10.1002/2014PA002758

Svensen, H., Corfu, F., Polteau, S., Hammer, Ø., & Planke, S. (2012). Rapid magma emplacement in the Karoo Large Igneous Province. *Earth and Planetary Science Letters*, *325–326*, 1–9. http://doi.org/10.1016/j.epsl.2012.01.015

Svensen, H., Planke, S., Chevallier, L., Malthe-Sørenssen, A., Corfu, F., & Jamtveit, B. (2007). Hydrothermal venting of greenhouse gases triggering Early Jurassic global warming. *Earth and Planetary Science Letters*, *256*(3–4), 554–566. http://doi.org/10.1016/j.epsl.2007.02.013

Them, T. R., Gill, B. C., Caruthers, A. H., Gröcke, D. R., Tulsky, E. T., Martindale, R. C., Smith, P. L. (2017). High-resolution carbon isotope records of the Toarcian Oceanic Anoxic Event (Early Jurassic) from North America and implications for the global drivers of the Toarcian carbon cycle. *Earth and Planetary Science Letters, 459*, 118-126.

Thibodeau, A. M., Ritterbush, K., Yager, J. A., West, A. J., Ibarra, Y., Bottjer, D. J., Corsetti, F. A. (2016). Mercury anomalies and the timing of biotic recovery following the end-Triassic mass extinction. *Nature Communications*, *7*, 11147. http://doi.org/10.1038/ncomms11147

Tišljar, J., Vlahovicć, I., Velić, I., Sokač, B. (2002). Carbonate platform megafacies of the Jurassic and Cretaceous deposits of the Karst Dinarides. *Geologia Croatica*, *55*(2), 139–170.

Trecalli, A., Spangenberg, J. E., Adatte, T., Föllmi, K. B., & Parente, M. (2012). Carbonate platform evidence of ocean acidification at the onset of the early Toarcian oceanic anoxic event. *Earth and Planetary Science Letters*, 357–358.

Tribovillard, N., Algeo, T. J., Lyons, T., & Riboulleau, A. (2006). Trace metals as paleoredox and paleoproductivity proxies: An update. *Chemical Geology*, *232*(1–2), 12–32. http://doi.org/10.1016/j.chemgeo.2006.02.012

Turnšek D., Buser S. & Debeljak I. (2003). Liassic coral patch reef above the "Lithiotid limestone" on Trnovski gozd plateau, west Slovenia. *Razprave IV. razreda SAZU, 44*, 29-49.

Vahrenkamp, V., Franco, B. J., Popa, D., Barata, J., Dhabi, A., For, C., Bulot, L. (2015). Development and Infill of the Late Albian to Turonian Shilaif Intrashelf Basin at the Eastern Margin of the Giant Mesozoic Arabian Carbonate Platform: Basin Architecture and Time Stratigraphy. *International Petroleum Technology Conference, 18488-MS*.

Van Buchem, F. S. P., Razin, P., Homewood, P. W., Oterdoom, W. H., & Philip, J. (2002). Stratigraphic organization of carbonate ramps and organic- rich intrashelf basins: Natih Formation (middle Cretaceous) of northern Oman. *AAPG Bulletin*, *86*(1), 21–53.

Van de Schootbrugge, B., Bachan, A., Suan, G., Richoz, S., & Payne, J. L. (2013). Microbes, mud and methane: Cause and consequence of recurrent early Jurassic anoxia following the end-Triassic mass extinction. *Palaeontology*, *56*, 685–709. http://doi.org/10.1111/pala.12034

van der Plas, L. V. D., & Tobi, A. C. (1965). A chart for judging the reliability of point counting resuts. *American Journal of Science*. http://doi.org/10.2475/ajs.263.8.722

Vlahović, I., Tišljar, J., Velić, I., & Matičec, D. (2005). Evolution of the Adriatic Carbonate Platform: Palaeogeography, main events and depositional dynamics. *Palaeogeography, Palaeoclimatology, Palaeoecology*, *220*(3–4), 333–360. http://doi.org/10.1016/j.palaeo.2005.01.011

Weissert, H., & Erba, E. (2004). Volcanism, CO_2 and palaeoclimate: a Late Jurassic-Early Cretaceous carbon and oxygen isotope record. *Journal of the Geological Society*, *161*(4), 695–702. http://doi.org/10.1144/0016-764903-087

Weissert, H., Lini, A., Föllmi, K. B., & Kuhn, O. (1998). Correlation of Early Cretaceous carbon isotope stratigraphy and platform drowning events: a possible link? *Palaeogeography, Palaeoclimatology, Palaeoecology*, *137*(3–4), 189–203. http://doi.org/10.1016/S0031-0182(97)00109-0

Wilkin, R. T., Barnes, H. L., & Brantley, S. L. (1996). The size distribution of framboidal pyrite in modern sediments: An indicator of redox conditions. *Geochimica et Cosmochimica Acta*, *60*(20), 3897–3912. http://doi.org/10.1016/0016-7037(96)00209-8

Winterer, E. L., & Bosellini, A. (1981). Subsidence and sedimentation on the Jurassic continental margin, southern Alps, Italy. *American Association of Petroleum Geologists Bulletin*, *65*(21), 394–421.

Woodfine, R. G., Jenkyns, H. C., Sarti, M., Baroncini, F., & Violante, C. (2008). The response of two Tethyan carbonate platforms to the early Toarcian (Jurassic) oceanic anoxic event: environmental change and differential subsidence. *Sedimentology*, *55*, 1011–1028. http://doi.org/10.1111/j.1365-3091.2007.00934.x

Wrigley, R., Hodgson, N., & Esestime, P. (2015). Petroleum geology and hydrocarbon potential of the Adriatic Basin, offshore Croatia. *Journal of Petroleum Geology*, *38*, 301–316.

Zhang, Y., Pe-Piper, G., & Piper, D. J. W. (2014). Sediment geochemistry as a provenance indicator: Unravelling the cryptic signatures of polycyclic sources, climate change, tectonism and volcanism. *Sedimentology*, *61*(2), 383–410. http://doi.org/10.1111/sed.12066